



## OPEN ACCESS

## EDITED BY

Yi Zheng,  
Sun Yat-sen University, China

## REVIEWED BY

Jinchao Wu,  
China University of Geosciences (Beijing)  
Energy Institute, China  
Xi Wang,  
Jilin University, China

## \*CORRESPONDENCE

Hai-Xiang Zhao,  
✉ zhaohx@hhu.edu.cn

RECEIVED 31 October 2025

REVISED 18 December 2025

ACCEPTED 29 December 2025

PUBLISHED 15 January 2026

## CITATION

Huang R-H, Zhao H-X, Wang J-X and  
Zhang C-L (2026) Ore genesis of the large  
Luobugaizi lead-zinc deposit in Xinjiang, NW  
China: constrains from lead isotope, *in-situ*  
trace elements and sulfur isotope of sulfides.  
*Front. Earth Sci.* 13:1736494.  
doi: 10.3389/feart.2025.1736494

## COPYRIGHT

© 2026 Huang, Zhao, Wang and Zhang. This  
is an open-access article distributed under  
the terms of the [Creative Commons  
Attribution License \(CC BY\)](https://creativecommons.org/licenses/by/4.0/). The use,  
distribution or reproduction in other forums is  
permitted, provided the original author(s) and  
the copyright owner(s) are credited and that  
the original publication in this journal is cited,  
in accordance with accepted academic  
practice. No use, distribution or reproduction  
is permitted which does not comply with  
these terms.

# Ore genesis of the large Luobugaizi lead-zinc deposit in Xinjiang, NW China: constrains from lead isotope, *in-situ* trace elements and sulfur isotope of sulfides

Rui-Hong Huang<sup>1</sup>, Hai-Xiang Zhao<sup>1\*</sup>, Jia-Xin Wang<sup>2</sup> and  
Chuan-Lin Zhang<sup>3</sup>

<sup>1</sup>School of Earth Sciences and Engineering, Hohai University, Nanjing, China, <sup>2</sup>Chengdu Xinli Geological Exploration Co., Ltd., Chengdu, China, <sup>3</sup>College of Oceanography, Hohai University, Nanjing, China

The recently discovered large Luobugaizi Pb-Zn deposit, located at the junction of the South Pamir and Karakoram Mountains, is a key component of the West Kunlun–Karakoram Pb-Zn Metallogenic Belt. Mineralization occurs mainly within the clastic rocks of the Silurian Wenquangou Formation, with ore minerals dominated by sphalerite and galena. This study focuses on the chemical composition of sphalerite and S-Pb isotopic characteristics of sulfides from the deposit to constrain its mineralization temperature, elemental substitution mechanisms, and metal sources. Sphalerite at Luobugaizi is characterized by relatively high concentration of Fe, Mn, Cd, Co and Sb, and relatively low concentration of Ge, Ag, In and As. Several elements, including Fe, Co, Cu, Ag, Ga, Ge, and In, substitute into the sphalerite lattice. Given the temperature-dependent nature of sphalerite trace element contents, it serves as a reliable geothermometer. The formation temperature of sphalerite was calculated using three distinct methods (Fe/Zn, GGIMF, and SPRFT software), with the average values ranging from 195 °C to 257 °C, indicating low-medium temperature hydrothermal conditions. The  $\delta^{34}\text{S}_{\text{V-CDT}}$  values of sphalerite range from  $-1.2\%$  to  $+3.3\%$ , suggesting a magmatic-hydrothermal sulfur source. Lead isotope compositions of sulfides ( $^{206}\text{Pb}/^{204}\text{Pb} = 18.41\text{--}18.44$ ;  $^{207}\text{Pb}/^{204}\text{Pb} = 15.70\text{--}15.71$ ;  $^{208}\text{Pb}/^{204}\text{Pb} = 38.70\text{--}38.76$ ) are identical to those of local Cretaceous granitoids, which are considered a potential metal source. Crucially, published geochronological data indicate that the emplacement ages of these granitoids are consistent with the mineralization age of the Luobugaizi deposit. These granitoids were interpreted in previous studies as products of crust-mantle interaction during the northward subduction of the Tethyan oceanic slab. Therefore, we propose that the metals were likely sourced from a coeval magmatic system related to these granitoids and were deposited by magmatic-hydrothermal fluids in fractures of the clastic sequence. Integrated evidence classifies

the Luobugaizi deposit as a magmatic-related, low-to medium-temperature hydrothermal system.

#### KEYWORDS

Luobugaizi lead-zinc deposit, mineralization temperature, sources of ore-forming material, subduction of Tethyan oceanic slab, sulfur and lead isotopes, trace element

## 1 Introduction

The West Kunlun-Karakoram Pb-Zn mineralization belt, on the southwestern Tarim Basin, spans the Hetian, Tianshuihai, Kudi and Tashkurgan regions and encompasses the West Kunlun Qiao'er-Tianshan mineralization area (Wang et al., 2021). The mineralized area hosts key mineral deposits, including the Dahongliutan Li-Be deposit, giant Huoshaoyun Pb-Zn deposit, Zankan super-large iron deposit, and the Malkansu manganese deposit (Qiao et al., 2015; Li et al., 2019; Zhang B. L. et al., 2020; Hong et al., 2025). The recently discovered large Luobugaizi Pb-Zn deposit is also regarded as a component of this mineralization area (Figure 1; Jiang et al., 2024).

Recent research in this mineralization zone has made significant advances in understanding the origin of ore-forming materials, the source and characteristics of mineralizing fluids, and the enrichment patterns of associated critical elements (Dong et al., 2006; Yan et al., 2012; Xu et al., 2013; Zhang et al., 2014; Qiao et al., 2021). However, the large Luobugaizi Pb-Zn deposit, located on the southwestern edge of the Mingtiegai sub-district in the West Kunlun-Qiao'er Tianshan mineralization area, has received limited attention. The genesis of this deposit remains poorly constrained. Based on previous studies on geochronology, researchers have proposed that the deposit is coeval with the Cretaceous granites in the region, and thus classified as a magmatic-hydrothermal deposit (Wang et al., 2021). However, to date, geochemical evidence regarding key aspects such as ore-forming temperatures and the sources of metallogenic materials is lacking. Therefore, further investigation is required to constrain the genetic model of the Luobugaizi deposit.

Sphalerite, a common mineral in Pb-Zn deposits, is rich in minor and trace elements, including Fe, Mn, Co, Cu, Ag, Cd, Ga, Ge, In, Sb and Bi (Cook et al., 2009). These elements offer insights into the deposit's origin (Pfaff et al., 2009; Cook et al., 2011; Zhuang et al., 2019). Additionally, sphalerite, a common geothermometer, is often used to constrain the mineralization temperature of the deposit (Zhang, 1987; Cook et al., 2009; Ye et al., 2011; Keith et al., 2014; Zhang J. K. et al., 2022; Zhao et al., 2024). Sulfur isotopes are invaluable for tracing mineral origins, especially in hydrothermal mineralization studies (Ohmoto, 1972; Ault, 2004; Zhou J. et al., 2013; Bao et al., 2017; Faisal et al., 2022). Pb isotopes serve as a powerful tracer for the origin of metals in hydrothermal systems. The characteristic ratios of different reservoirs (e.g., mantle, upper crust, orogenic belt) enable researchers to identify potential sources (Zartman and Doe, 1981; Shen et al., 2007; Zeng et al., 2014; Ding et al., 2016; Gill et al., 2019; Zhang H. S. et al., 2020; Zhu et al., 2020; Yang F. C. et al., 2024). Furthermore, recent advances in laser ablation inductively coupled plasma mass spectrometry (LA-ICP-MS) technology now allow for high-resolution, micro-area, *in-situ*

analysis of sulfides (Chen et al., 2017). This enables more precise tracking of ore-forming substance origins and better reveals metal enrichment mechanisms (Mason et al., 2006; Yuan H. L. et al., 2018).

In this study, we performed detailed mineralogical observations of Pb-Zn ores from the Luobugaizi Pb-Zn deposit, Xinjiang. We conducted *in-situ* LA-ICP-MS analysis of sphalerite trace elements, *in-situ* S isotope of sphalerite using laser ablation multi-collector inductively coupled plasma mass spectrometry (LA-MC-ICP-MS), and Pb isotope of sulfides, in order to constrain the origin of the mineralizing material, the mineralization temperature, explore element enrichment and replacement mechanisms, and finally identify the deposit's genesis.

## 2 Geological background

### 2.1 Regional geology

The West Kunlun-Karakoram orogen is divided into the North Kunlun (NKT), South Kunlun (SKT) and Tianshuihai tectonic units (Xiao et al., 2005; Wang et al., 2014; Wang et al., 2017) (Figure 1A). The Luobugaizi Pb-Zn deposit occurs in a rift basin within the Mingtiegai landmass (second-order tectonic unit), which lies on the northern margin of the ancient Tethys tectonic domain, the junction of the South Pamir and the Karakoram Mountains. Stratigraphically, the region belongs to the Qiangbei-Changdu-Simao zone, specifically the Mingtiegai subzone. The exposed strata mainly comprise the Paleoproterozoic Bulunkole Group (Pt<sub>1</sub>B) medium-to high-grade metamorphic rocks, the Lower Silurian Wenquangou Formation (S<sub>1</sub>w) fine-grained clastic rocks and limestone, the Carboniferous Qatir Group (C<sub>2</sub>Q) carbonate, the Jurassic Longshan Formation (J<sub>1-2</sub>L) marble and pyroclastic rocks, and Quaternary (Q) sediments (Figure 1B). The Palaeozoic strata are widespread in the Mingtiegai area, while the Mesozoic and Cenozoic strata occur over limited areas. Besides the Luobugaizi Pb-Zn deposit, the region hosts other deposits, such as the Tuokemansu tungsten deposit, peripheral Pb-Zn and copper occurrences around Luobugaizi, the Qunsagiriya copper and Pb-Zn, the Dasdarnan Pb-Zn, the Athiyayile copper and the Dabalama hematite deposits.

The region experienced intense regional tectonic activity. Major regional faults include the NW-NNW-trending Kangxiwa fault (F1, Figure 1A), the NW-trending Taaxi fault (F2), the Tashkurgan fault (F3) and the SE-trending Dabudaer reverse fault (F4). Third-level tectonic faults include the NW-EW-trending Qunsaragiriya Fault (F5), the NW-trending Talisike fault (F6), the NW-trending Kizilekemu fault (F7) and the NW-trending Athiyayile fault (F8, Figure 1B).

Magmatic rocks are widely distributed across the region. Major regional magmatic rocks include Carboniferous granitoids, Early

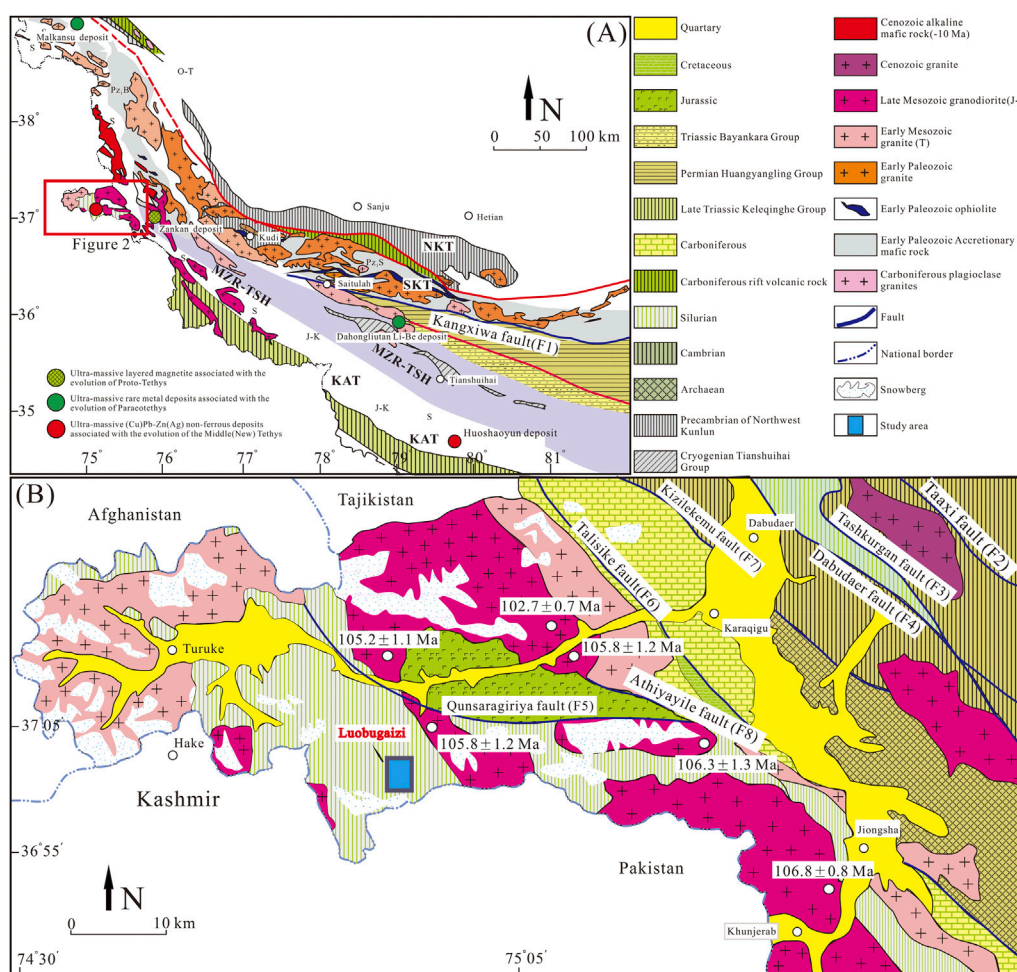


**FIGURE 1** (A) Simplified geologic map and distribution diagram of major mineral resources of the West Kunlun-Karakoram region (modified after Wang et al., 2021). (B) Regional geological map of Mingtiegai Subzone (modified after Wang et al., 2021). Cretaceous granite age data from Liu et al. (2020a). NKT: North Kunlun Tectonic, SKT: South Kunlun Tectonic, KAT: Karakoram Kunlun Tectonic, MZR-TSH: Mazha-Tianshuihai Tectonic.

Paleozoic volcanic rocks (530–450 Ma; Quek, 2018), Early Mesozoic granite (Triassic, 240–200 Ma; Liu et al., 2020b), Late Yanshanian intermediate-felsic intrusive rocks and Cenozoic alkaline mafic rocks. In the vicinity of the study area and within it, Late Yanshanian intermediate-felsic intrusive rocks are predominantly distributed (Figure 1B), which may be closely related to Pb-Zn mineralization.

## 2.2 Ore deposit geology

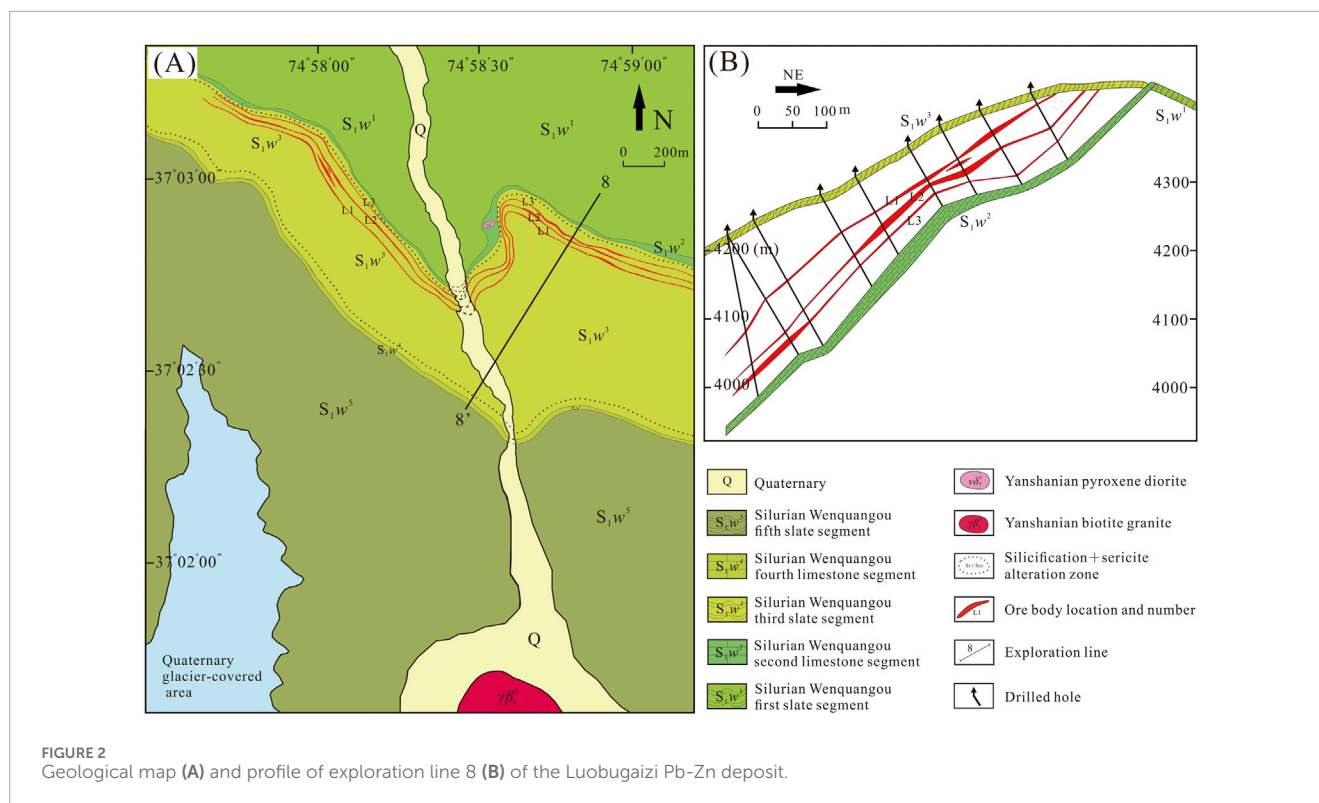
The exposed strata at the Luobugaizi Pb-Zn deposit are predominantly (95%) composed of the Lower Silurian Wenquangou Formation ( $S_1w$ ), a shallowly metamorphosed sandstone-shale sequence. This Formation is divided into five lithologic members, with the third member ( $S_1w^3$ , predominantly slate) serving as the primary ore-hosting layer. Quaternary deposits cover the remaining ~5% of the surface (Figure 2).

The deposit is structurally controlled by the NW- to EW-trending Qunsaragiriya Fault (F5, Figure 1B), which separates

the Yanshanian granodiorite to the south from Jurassic strata to the north. Yanshanian intermediate-felsic intrusive rocks are distributed approximately 2.5 km east of the deposit and also occur within its southern sector (Figures 1, 2A). These intrusions occur predominantly as stocks and consist mainly of granodiorite, quartz diorite and biotite granite.

The deposit comprises nine individual orebodies, with total resources exceeding one million tonnes (Wang et al., 2021). The orebodies occur primarily in stratiform, sub-stratiform and lenticular shapes. While some orebodies conform to the attitude of the surrounding strata, other Pb-Zn veins crosscut or displace the original bedding planes (Figure 2B). Weighted average grades are 2.30% Pb and 3.21% Zn, with a combined Pb + Zn grade of 5.51%, meeting industrial standards. Furthermore, the deposit contains associated elements such as Ag, Cd, and Ga.

The ore deposit has a relatively simple mineral assemblage. The major ore minerals are sphalerite and galena, accompanied by pyrite, chalcopyrite, siderite, cerussite, tetrahedrite, covellite and limonite. Gangue minerals include quartz, sericite, clay minerals,



calcite, plagioclase, chlorite, graphite and organic carbon. Ore structures include massive, blocky, angular breccia, and veinlet-like types (Figures 3A–F). The ores mainly show euhedral to subhedral granular, replacement, metasomatic, intergranular, heteromorphic, and exsolution textures (Figures 4A–F). The mineral assemblage was predominantly formed during the hydrothermal mineralization period, with siderite and cerussite being minor products of subsequent supergene alteration.

Under microscopic observation, pyrite is commonly paragenetic with quartz and is enclosed by sphalerite (Figure 4D). Both in hand specimens and under the microscope, sphalerite veins can be clearly observed to be crosscut by galena-quartz veins (Figures 3E, 4B,F), whereas the quartz-carbonate veins, representing the latest mineralization stage, crosscut either sphalerite veins or galena veins (Figures 3A,D). Based on these observations, the hydrothermal mineralization of this deposit can be divided into four stages (Figure 5). Stage 1 is the quartz-pyrite stage characterized by quartz-sericite assemblage with intergrown pyrite. Stage 2 is the quartz-sphalerite-carbonate stage. It is dominated by sphalerite precipitation, with minor pyrite-chalcopryrite-galena. Sphalerite is yellowish-brown in hand specimens, dark to brownish-grey in reflected light, and sometimes shows “chalcopryrite disease” (Figure 4A). Stage 3 is the quartz-galena-carbonate stage. Ore minerals include galena, chalcopryrite and trace sphalerite. Galena veins are observed to crosscut sphalerite (Figure 4E). Stage 4 is the quartz-carbonate stage. It represents the latest hydrothermal phase, characterized by the formation of quartz and calcite, interspersed with minerals from earlier stages.

Alteration is dominated by silicification and sericitization, with subordinate dolomitization, carbonatization and chloritization. Silicification and sericite alteration are well developed and most

evident in the surrounding rock of Pb-Zn orebodies. Supergene alteration produces cerussite and smithsonite, which are vivid red or orange-yellow, making them key exploration indicators.

## 3 Sample preparation and analytical methods

### 3.1 Sample preparation

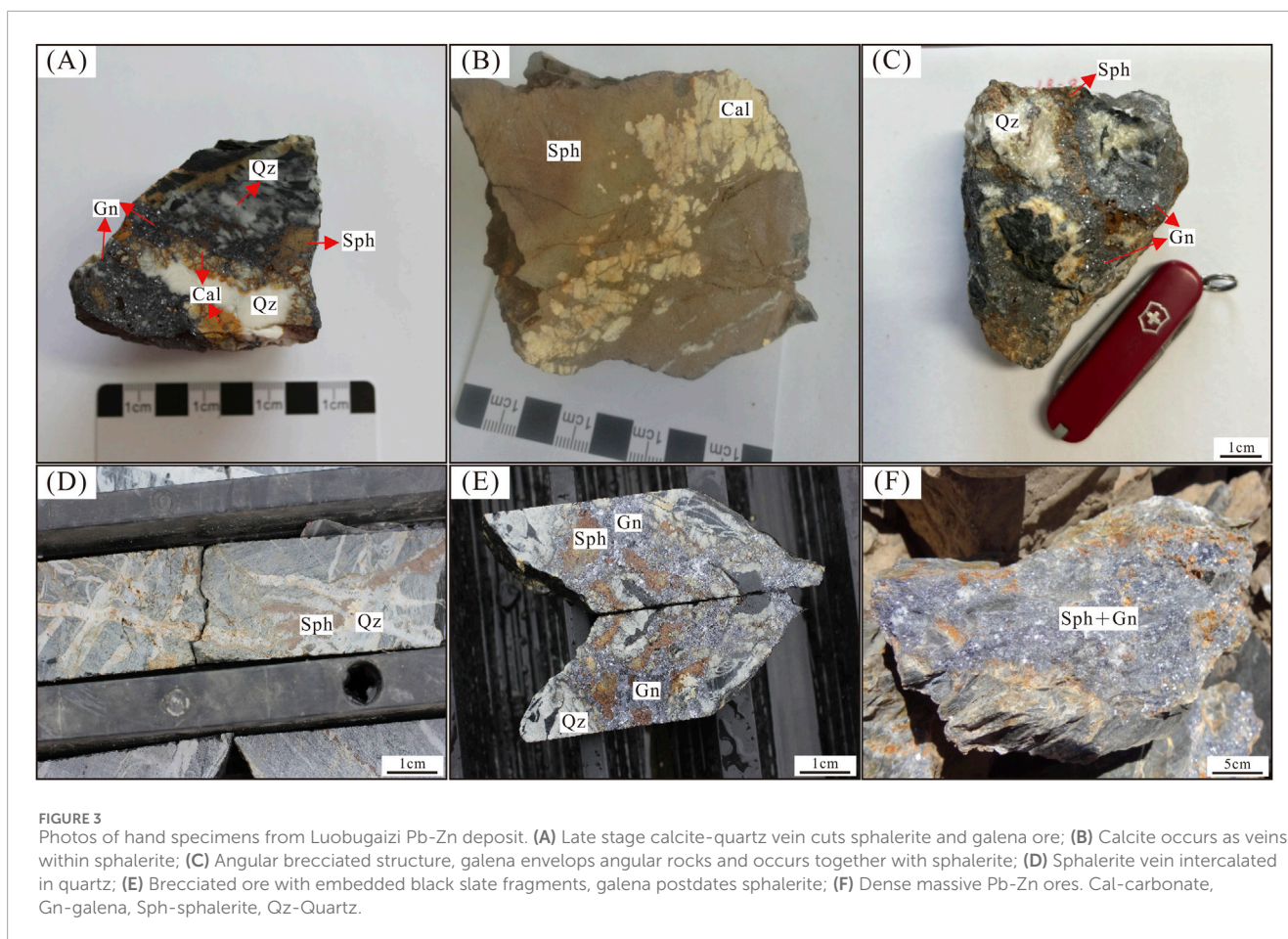
In this study, ten representative samples were collected from the initial mining area (eastern mining zone) of the Luobugaizi Pb-Zn deposit. These samples were prepared as polished thin sections for optical microscopic examination to characterize their mineralogy and paragenetic relationships. To guide precise spot selection for *in situ* analysis, micrographs at multiple scales were first acquired for all samples. These images ensured that measurement points on sphalerite grains were accurately targeted for subsequent *in situ* trace element (LA-ICP-MS) and S isotope (LA-MC-ICP-MS) analysis.

Separately, individual sphalerite and galena grains were hand-picked from eight ore samples for Pb isotope analysis.

### 3.2 Analytical methods

#### 3.2.1 Trace element analysis

*In situ* trace element analysis of sphalerite was conducted by LA-ICP-MS at Nanjing FocuMS Technology Co. Ltd, using a Teledyne Cetac Analyte Excite laser-ablation system coupled with an Agilent 7700x quadrupole ICP-MS. The 193 nm ArF excimer laser was operated at 3.0 J/cm<sup>2</sup>. Each analysis comprised 20 s of background



measurement (gas blank) and 40 s of sample ablation. Ablation was performed using a laser spot size of 40  $\mu\text{m}$  at a repetition rate of 6 Hz. Helium (370 mL/min) served as the carrier gas to efficiently transport the ablated aerosol from the cell, which was then mixed with argon ( $\sim 1.15$  L/min) prior to its introduction into the ICP torch.

The USGS polymetallic sulfide pressed-powder pellet MASS-1 and the synthetic basaltic glasses reference material GSE-1G were used for external calibration.

### 3.2.2 Sulfur isotope analysis

*In situ* sulfur isotope analysis was conducted on sphalerite using laser ablation MC-ICP-MS at the State Key Laboratory of Critical Earth Material Cycling and Mineral Deposits, Nanjing University (Nanjing, China). Galena was not analyzed to avoid Pb contamination of the instrument.

The analytical system consisted of a GeolasPro ArF excimer (193 nm) laser ablation coupled with the Neptune plus MC-ICP-MS. Argon (850 mL/min) and He (700 mL/min) were used as auxiliary and carrier gases, respectively. All measurements were conducted with a spot size of  $\sim 30$   $\mu\text{m}$ , a repetition rate of 6 Hz and a laser energy of 4 J/cm<sup>2</sup>. Each analysis lasted 60 s, including a 5 s pre-ablation background measurement, a 50 s data acquisition interval and a 5 s washout period. Cup configuration for sulfur was H3 and C for <sup>34</sup>S and <sup>32</sup>S, respectively. Mass resolution was set at 4,000 to avoid isobaric interferences.

All  $\delta^{34}\text{S}$  values are reported relative to the Vienna Canyon Diablo Troilite (V-CDT) standard. Instrumental drift and mass bias were corrected using the standard-sample bracketing (SSB) method. The WS-1 pyrite standard ( $\delta^{34}\text{S} = 1.1 \pm 0.2\text{‰}$ , 2SD; Zhu et al., 2016) was used for calibration and NBS123 sphalerite for quality control ( $\delta^{34}\text{S} = 17.1\text{‰} \pm 0.2\text{‰}$ , 2SD). The analytical uncertainty was generally better than 1.0‰ (2SD).

### 3.2.3 Lead isotope analysis

High precision Pb isotope measurements were carried out at Nanjing FocuMS Technology Co. Ltd. Sulfide powders were digested in a mixture of 0.4 mL concentrated HNO<sub>3</sub> and 1.0 mL concentrated HCl in screw-top beakers on a hotplate at 60 °C. After drying, residues were then redissolved in 1.5 mL of a 0.2 mol/L HBr + 0.5 mol/L HNO<sub>3</sub> mixture before ion exchange purification.

Pb was separated using Bio-Rad AG1-X8 anion exchange resin. Lithophile elements (Sr and REE) were initially washed out from the column with a 0.2 mol/L HBr + 0.5 mol/L HNO<sub>3</sub> mixture, followed by Pb collection with Milli-Q water. A second column step was applied to improve purity. The purified Pb fraction was dried down and dissolved in 1.0 mL 2% HNO<sub>3</sub>.

Pb concentrations were determined using an Agilent 7700x quadrupole ICP-MS. Based on these results, the purified solutions were appropriately diluted to  $\sim 40$  ppb Pb (with 10 ppb Tl added as an internal standard) and introduced into Nu Plasma II MC-ICP-MS through Aridus II desolvating nebulizer system.

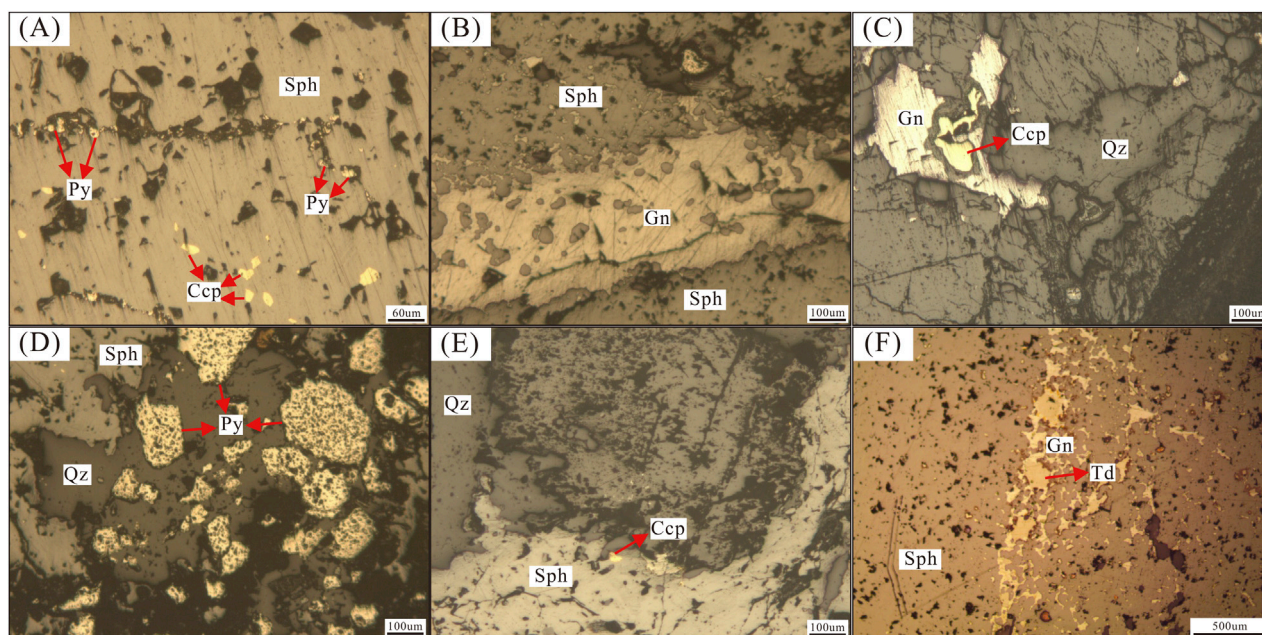


**FIGURE 4** Microphotographs of ores from Luobugaizi Pb-Zn deposit (reflected light). (A) “Chalcopyrite disease” texture in spherulite and pyrite in spherulite fractures; (B) Galena veins are observed in spherulite; (C) Coarse chalcopyrite and galena grains occur irregularly in quartz; (D) semi-self-shaped pyrite coexists with quartz in spherulite; (E) Spherulite occurs as massive aggregates and forms irregular to regular intergrowths with non-metallic minerals. Fine-grained chalcopyrite is dissolved within it; (F) Galena and tetrahedrite occur as bands within spherulite. Qz-Quartz, Sph-Sphalerite, Py-Pyrite, Ccp-Chalcopyrite, Td-Tetrahedrite.

Stage Mineral	Quartz-pyrite stage	Quartz-sphalerite -carbonate stage	Quartz-galena -carbonate stage	Quartz-carbonate stage
Sericite	Major			
Calcite		Major		
Quartz	Major	Major	Major	Major
Pyrite	Major	Trace		
Chalcopyrite		Trace		
Sphalerite		Major	Trace	
Galena		Trace	Major	
Tetrahedrite			Major	

major    
  minor    
  trace

**FIGURE 5** The paragenetic sequence of minerals in the Luobugaizi Pb-Zn deposit.

Raw data of Pb isotopic ratios were internally corrected for mass bias by normalizing to  $^{205}\text{Tl}/^{203}\text{Tl} = 2.3885$  with exponential law. Instrumental drift was monitored by repeated analysis of NIST SRM 981. Geochemical reference materials USGS BCR-2, BHVO-2, AGV-2, RGM-2 were treated as quality controls.

## 4 Results

### 4.1 Trace elements in sphalerite

The trace element compositions of sphalerite from the Luobugaizi Pb-Zn deposit are summarized in [Table 1](#).

TABLE 1 Analysis results of trace elements in sphalerite from Luobugaizi Pb-Zn deposit.

Sample number	Fe/%	Zn/%	Ga	Ge	Cd	In	Ag	Pb	Cu	Mn	Co	Ni	As	Se	Sn	Sb
lb17-2-1sph	0.59	70.1	46.9	-	1,080	23.3	15.5	15,107	71.7	37.7	19.1	2.81	-	1.63	0.79	56.7
lb17-2-2sph	0.55	70.5	390	50.2	1,085	26.7	181	56.5	2,780	25.5	14.7	4.18	68.6	1.65	1.34	2,672
lb17-1sph	2.15	69.6	121	1.16	1,593	194	6.56	63.3	211	45.4	54.6	1.47	3.56	-	0.71	20.4
lb17-3-1sph	3.20	67.7	56.0	20.2	1802	237	7.45	33.4	185	35.8	87.6	4.60	34.9	1.27	2.19	42.6
lb14-1-1sph	3.05	69.6	84.2	0.53	1721	90.3	1.68	10.2	125	23.3	58.4	2.74	2.46	1.19	0.60	14.4
lb14-1-2sph	3.02	69.7	74.4	16.1	1710	46.2	1.98	16.4	102	22.6	57.9	4.12	12.5	-	0.62	29.8
lb14-2-1sph	2.56	69.7	55.8	1.81	1,640	1.36	0.92	4.11	53.6	59.8	41.0	6.07	4.06	0.94	0.20	5.67
lb18-1-1sph	1.85	71.1	15.8	6.23	1,019	37.4	9.62	-	61.8	56.1	53.7	1.33	-	1.26	-	21.8
lb18-2-1sph	1.93	71.1	16.3	2.27	1,198	17.1	11.8	30.4	47.1	64.2	53.0	1.44	-	-	0.35	42.5
lb18-3-1sph	1.93	68.9	23.3	0.36	1,167	41.5	20.6	25,798	49.9	61.2	56.1	1.74	2.06	1.15	0.28	63.5
lb23-1-1sph	2.85	70.0	19.3	1.71	1,168	7.54	10.2	1,575	152	149	46.8	2.45	-	1.73	0.39	45.6
lb23-1-5sph	2.79	68.7	3.6	-	1,077	14.5	10.5	485	221	431	63.9	1.46	-	1.31	-	31.0
lb23-3-3sph	2.41	70.0	17.0	-	1,092	11.2	2.69	8.11	32.9	80.0	63.6	6.22	1.95	-	0.33	4.90
lb23-4-2sph	2.56	69.6	20.5	24.9	1,126	4.95	7.70	133	36.8	94.0	47.9	4.57	19.5	0.77	0.29	26.8
lb23-5-1sph	2.84	69.3	20.1	0.26	1,045	37.5	4.13	36.4	62.1	61.5	58.1	2.82	-	-	0.18	14.9
lb25-1-1sph	4.25	67.1	1.45	-	972	1.27	1.03	2.84	4.16	23.6	66.7	0.14	2.57	2.06	0.27	1.09
lb25-2sph	3.83	67.1	2.31	5.11	906	0.48	6.15	14.5	8.58	75.1	39.9	0.53	-	1.39	0.20	11.7
lb25-3-1sph	3.65	68.3	0.64	-	915	0.56	1.54	4.16	2.89	27.6	43.8	0.42	-	1.03	0.19	2.37
lb25-3-3sph	3.59	66.3	0.69	-	917	0.65	2.23	2.05	5.86	30.9	42.5	0.37	-	-	-	2.87
lb31-1-1sph	3.53	67.6	108	14.4	1926	12.7	1.09	3.66	114	25.8	69.3	3.04	6.65	1.66	0.26	65.4
lb31-2sph	2.56	68.8	36.1	-	1,688	2.80	1.97	9.01	57.1	37.4	32.1	2.34	2.60	-	0.18	12.8
lb31-3sph	1.94	69.1	17.2	7.20	1,302	0.01	1.06	4.04	20.0	10.1	24.1	1.37	-	1.13	0.15	8.80
lb-3-1sph	1.75	69.0	13.3	1.01	1,428	0.03	3.87	14.6	19.0	94.1	27.9	12.4	12.5	1.25	0.10	14.4

(Continued on the following page)

TABLE 1 (Continued) Analysis results of trace elements in sphalerite from Luobugaizi Pb-Zn deposit.

Sample number	Fe/%	Zn/%	Ga	Ge	Cd	In	Ag	Pb	Cu	Mn	Co	Ni	As	Se	Sn	Sb
lb3-2sph	2.11	68.4	20.0	-	1,278	2.14	2.39	8.36	20.7	112	30.1	5.34	-	1.52	0.27	5.21
lb-3-2sph2	2.14	68.3	12.0	-	1,280	1.77	1.96	335	13.6	107	30.0	4.66	2.30	1.44	0.16	3.51
lb3-2sph3	2.02	68.3	17.7	-	1,282	1.76	6.37	11.6	20.5	99.8	29.4	2.89	-	-	0.46	10.7
lb3-3-2sph	1.76	69.6	26.9	-	1,202	0.08	0.58	-	28.8	71.3	25.5	4.52	2.95	3.01	-	2.21
lb-5-1sph	3.80	67.2	36.4	2.22	1,176	0.06	0.97	3.04	38.3	30.4	45.7	1.70	2.48	1.55	0.21	4.19
lb5-2sph	3.47	67.3	68.6	36.5	1,075	0.32	1.62	5.16	72.9	31.6	65.3	2.13	3.93	1.18	0.35	6.76
lb5-3sph	2.38	68.3	6.45	0.53	1,040	0.00	3.86	98.7	20.4	38.7	43.0	1.29	-	2.03	0.41	35.3
lb6-1-2sph	2.95	66.6	51.7	0.59	1,505	152	25.9	141	133	65.1	65.1	9.82	20.8	-	-	36.4
lb6-1-3sph	2.87	67.2	46.9	-	1,433	144	2.23	3,003	118	68.5	59.7	4.09	2.50	1.99	0.20	4.43
lb6-2-1sph	2.40	67.7	95.9	0.44	1,356	133	6.58	5.68	160	70.8	57.2	4.10	2.05	-	-	8.16
lb6-3-1sph	1.72	67.5	25.9	5.82	1,349	0.13	16.2	104	51.4	65.4	19.5	4.13	2.87	-	0.22	39.5
lb8-1sph	3.40	66.4	142	42.7	926	2.39	7.66	-	149	48.2	25.9	0.83	-	-	-	97.4
lb8-2-1sph	3.16	67.4	3.77	0.50	1,261	0.76	2.51	11.5	31.8	64.0	21.4	0.76	2.19	-	0.22	11.0
lb8-3-1sph	3.47	67.0	16.2	-	931	19.2	0.75	40.4	25.3	53.6	22.5	0.86	-	-	-	0.70

“-” below the detection limit. All elements are in ppm except Fe and Zn.

Sphalerite contains low to moderate concentrations of Fe, ranging from 0.55% to 4.25%. Cadmium concentrations are high and relatively uniform (905–1925 ppm, mean 1,261 ppm), whereas Co concentrations are lower but also consistent (14.0–87.6 ppm, mean 44.9 ppm). Lead and Cu show the greatest concentration ranges (Pb: from below the detection limit up to 25,800 ppm, mean 1,388 ppm; Cu: 2.89–2,780 ppm, mean 143 ppm). Elements including Ge, Ga, In, Sb, and Ag demonstrate moderate concentrations that vary over one to two orders of magnitude (0–50.2 ppm, 0.64–390 ppm, 0–237 ppm, 0.70–2,672 ppm, and 0.58–181 ppm, respectively). Several elements are consistently present in low concentrations. Arsenic concentrations are generally low (1.95–68.6 ppm, mean 9.80 ppm), while elements like Ni, Se, and Sn are the least concentrated, with mean values all below 5 ppm.

## 4.2 Sulfur isotopes

The Sulfur isotope compositions of sphalerite are reported in Table 2 and Figure 6. The  $\delta^{34}\text{S}$  values for sphalerite range from  $-1.2\text{‰}$  to  $+3.3\text{‰}$  (mean  $+1.3\text{‰}$ ), exhibiting a relatively small variation compared to most sediment-hosted deposits. The values display a distinct “tower-like” distribution pattern, with the majority concentrated within a narrow peak between  $+1\text{‰}$  and  $+2\text{‰}$ .

## 4.3 Lead isotopes

The Pb isotopic compositions of sulfides from the Luobugaizi deposit are summarized in Table 3. The sulfides from the deposit have  $^{206}\text{Pb}/^{204}\text{Pb}$ ,  $^{207}\text{Pb}/^{204}\text{Pb}$ , and  $^{208}\text{Pb}/^{204}\text{Pb}$  values of 18.41–18.44 (mean 18.43), 15.70 to 15.71 (mean 15.70), and 38.70 to 38.76 (mean 38.74), respectively.

## 5 Discussion

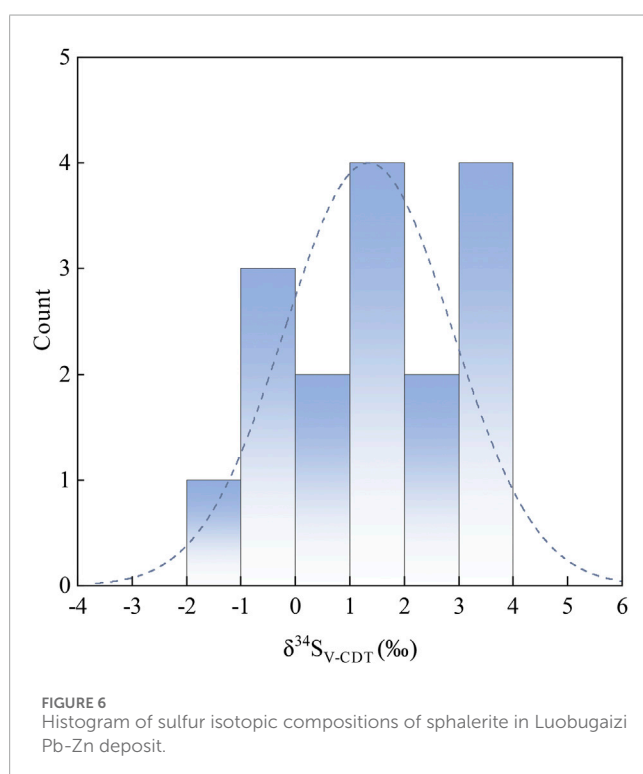
### 5.1 Substitution mechanism

The distribution of trace element concentrations in sulfides is controlled by their modes of occurrence. Numerous studies have shown that trace elements are incorporated into sulfides via various mechanisms, including homovalent substitution and as micro-inclusions of discrete minerals (Benedetto et al., 2005; Ciobanu et al., 2012; Reich et al., 2013; George et al., 2015; Yang et al., 2022). The investigation into the occurrence modes and substitution mechanisms of trace elements in sulfides is a prerequisite for using these elements to reconstruct the physicochemical conditions of deposit formation.

In sphalerite, the substitution of  $\text{Zn}^{2+}$  by minor/trace elements mainly occurs via simple or coupled substitution. Cations like  $\text{Fe}^{2+}$ ,  $\text{Cu}^{2+}$ ,  $\text{Mn}^{2+}$ ,  $\text{Cd}^{2+}$ , and  $\text{Co}^{2+}$ , which have similar ionic radius and charge to  $\text{Zn}^{2+}$ , can directly substitute

TABLE 2 S isotope compositions of sulfides in Luobugaizi Pb-Zn deposit.

Sample number	Mineral	$\delta^{34}\text{S}(\text{‰})$
lb18-1-1	Sphalerite	+1.7
lb18-2-1	Sphalerite	+3.3
lb18-3-1	Sphalerite	+2.2
lb17-3-1	Sphalerite	+3.1
lb17-2-1	Sphalerite	+0.4
lb17-2-2	Sphalerite	+1.7
lb17-1	Sphalerite	+3.3
lb25-3-2	Sphalerite	+1.3
lb23-4-2	Sphalerite	+1.8
lb23-5-1	Sphalerite	+3.2
lb23-1-2	Sphalerite	-0.4
lb23-1-1	Sphalerite	-0.7
lb23-6	Sphalerite	+2.1
lb23-3-3	Sphalerite	-1.2
lb25-1-1	Sphalerite	+0.1
lb25-2	Sphalerite	-0.4



( $\text{M}^{2+} \leftrightarrow \text{Zn}^{2+}$ ) into the crystal lattice (Cook et al., 2009; Lockington et al., 2014; Belissant et al., 2016; Babedi et al., 2019). In contrast, monovalent ( $\text{Cu}^+$ ,  $\text{Ag}^+$ ), trivalent ( $\text{As}^{3+}$ ,  $\text{Ga}^{3+}$ ,  $\text{Sb}^{3+}$ , and  $\text{In}^{3+}$ ) and tetravalent ( $\text{Sn}^{4+}$ ,  $\text{Ge}^{4+}$ ) cations with larger ionic radius are primarily incorporated via coupled substitution mechanisms (Cook et al., 2009; 2012; Ye et al., 2011; Bonnet et al., 2016; Li et al., 2020; Luo et al., 2022; Yang et al., 2022).

Binary plots show a generally negative correlation between Fe and Zn contents in sphalerite (Figure 7A), indicating a possible substitution of  $\text{Zn}^{2+}$  by  $\text{Fe}^{2+}$ . A weak positive correlation between Co and Fe (Figure 7B) implies that  $\text{Fe}^{2+}$  and  $\text{Co}^{2+}$  may jointly replace  $\text{Zn}^{2+}$ . In many Pb-Zn deposits, Ge and Ga in sphalerite show a correlation with Cu (Ye et al., 2016; Li et al., 2020; Zhang J. K. et al., 2022). Here, the strong positive correlation between Ga and Cu (Figure 7C) and the weak positive correlation between Ge and Cu (Figure 7D) indicate the following coupled substitutions:  $\text{Ga}^{3+} + \text{Cu}^+ \leftrightarrow 2\text{Zn}^{2+}$ ,  $\text{Ge}^{4+} + 2\text{Cu}^+ \leftrightarrow 3\text{Zn}^{2+}$ .

Trivalent cations  $\text{Sb}^{3+}$ ,  $\text{Sn}^{3+}$ , and  $\text{In}^{3+}$  are more likely to substitute  $\text{Zn}^{2+}$  via coupled substitution with monovalent cations  $\text{Cu}^+$  and  $\text{Ag}^+$  (Makovicky and Topa, 2015; Torró et al., 2022; Xiao et al., 2023). In the present study, the strong positive correlations observed between Sb and Cu (Figure 7E) and between Sb and Ag (Figure 7F) support the mechanisms:  $2\text{Zn}^{2+} \leftrightarrow \text{Cu}^+ + \text{Sb}^{3+}$  and  $2\text{Zn}^{2+} \leftrightarrow \text{Ag}^+ + \text{Sb}^{3+}$ . Similarly, the correlation between In and (Cu, Ag) (Figure 7H) can be explained by the substitution:  $\text{In}^{3+} + (\text{Cu}^+, \text{Ag}^+) \leftrightarrow 2\text{Zn}^{2+}$ .

Arsenic in sphalerite is typically present as  $\text{As}^{3+}$  (Yang et al., 2022; Li et al., 2024). The weak positive correlation between As and Cu (Figure 7G) suggests a possible coupled substitution of  $2\text{Zn}^{2+} \leftrightarrow \text{As}^{3+} + \text{Cu}^+$ . The strong positive correlation between Cu + Ag (monovalent cations) and Ga + As + Sb + Ge (tri- and tetravalent cations) (Figure 7I) implies that another substitution mechanism may exist:  $(\text{Cu}, \text{Ag})^{++} + (\text{Ga}, \text{As}, \text{Sb})^{3+} + \text{Ge}^{4+} \leftrightarrow 4\text{Zn}^{2+}$ .

## 5.2 Temperature

The concentrations of key trace elements in sphalerite (e.g., Fe, Mn, Co, Cd, In, Ga, Ge) are widely recognized as sensitive indicators of mineralization temperature (Möller, 1985; Frenzel et al., 2016; Frenzel et al., 2022; Bauer et al., 2019b; Xing et al., 2021). Sphalerite associated with high-temperature or magmatic-hydrothermal fluids generally has high Fe, In, Mn, and Se concentrations but low Ga, Ge, and Ti concentrations, exhibiting low Ga/In and Ge/In ratios (Frenzel et al., 2016; Bauer et al., 2019a; Li et al., 2022; Liu et al., 2025). In contrast, medium-temperature sphalerite commonly shows high Cd and In concentrations, with Ga/In ratios of 0.01–5 and Cd/Fe ratios of 0.02–1 (Li et al., 2022; Sun et al., 2023; Liu et al., 2025). Low-temperature sphalerite is typically lighter in colour and has relatively high Ga, Ge and Cd concentrations, with a Ga/In ratio ranging from 1 to 100 and elevated Ge/In values (Ye et al., 2011; Cook et al., 2012; Zhuang et al., 2019; Hu et al., 2021).

Sphalerite from Luobugaizi is typically light in colour and contains 1.71–4.25 wt% Fe, which is below the typical threshold for high-temperature sphalerite ( $\text{Fe} > 10\%$ ). The Ge content in sphalerite systematically increases with declining mineralization temperature. High-temperature sphalerite generally contains < 5 ppm Ge, medium-temperature sphalerite contains 5–50 ppm Ge,

TABLE 3 Pb isotope compositions of sulfides in Luobugaizi Pb-Zn deposit.

Sample number	Mineral	$^{206}\text{Pb}/^{204}\text{Pb}$	$^{207}\text{Pb}/^{204}\text{Pb}$	$^{208}\text{Pb}/^{204}\text{Pb}$
LB-3	Sphalerite	18.43	15.70	38.74
LB-3	Galena	18.43	15.71	38.75
LB-7	Sphalerite	18.43	15.70	38.73
LB-7	Galena	18.44	15.71	38.76
LB-8	Sphalerite	18.43	15.70	38.74
LB-8	Galena	18.43	15.70	38.74
LB-16	Sphalerite	18.42	15.71	38.74
LB-16	Galena	18.41	15.70	38.70
LB-22	Galena	18.43	15.70	38.73
LB-24	Sphalerite	18.42	15.70	38.72
LB-30	Galena	18.43	15.70	38.74
LB-31	Sphalerite	18.43	15.71	38.74

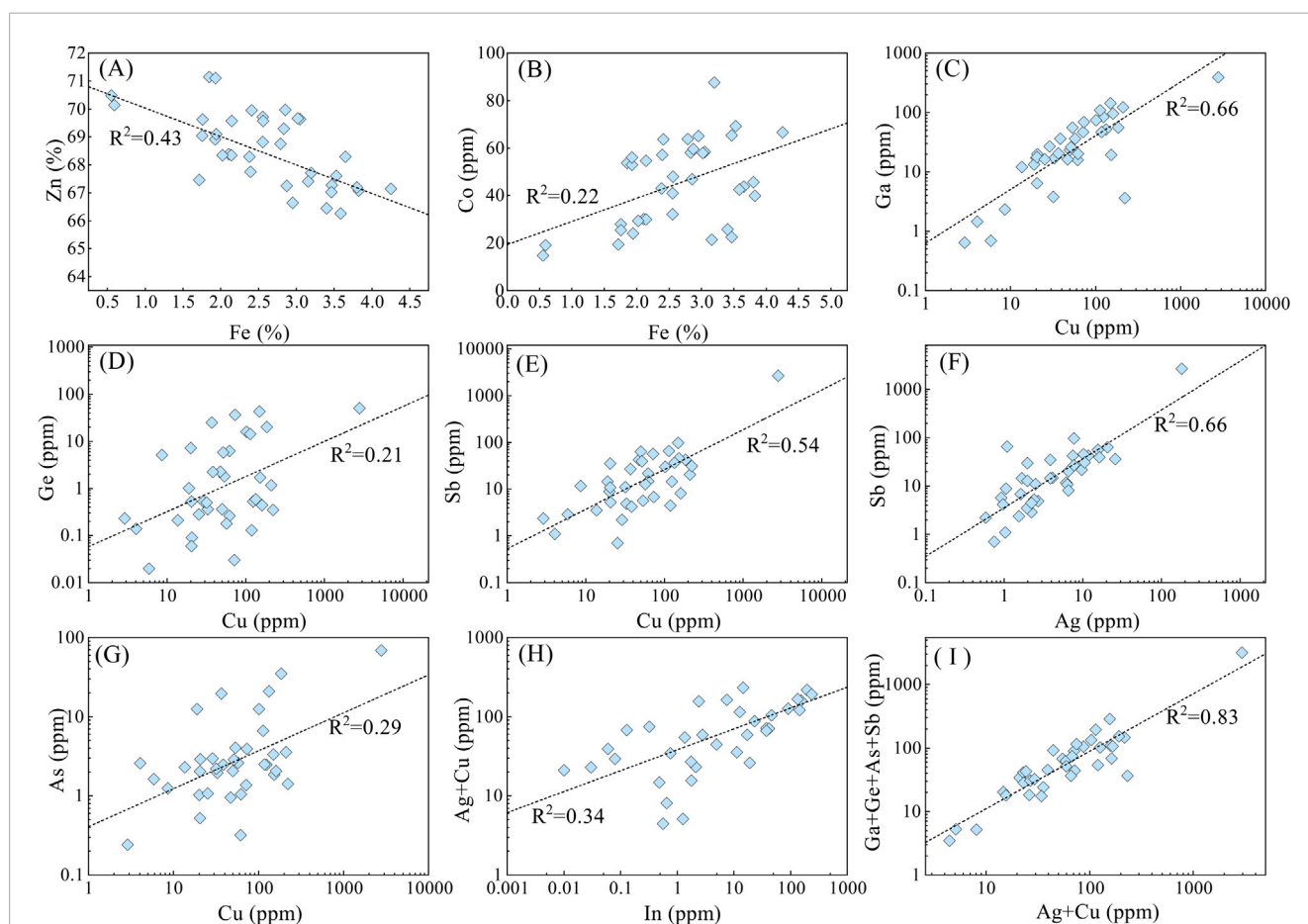


FIGURE 7 Correlation diagram of trace elements in sphalerite from Luobugaizi Pb-Zn deposit. (A) Zn vs. Fe; (B) Co vs. Fe; (C) Ga vs. Cu; (D) Ge vs. Cu; (E) Sb vs. Cu; (F) Sb vs. Ag; (G) As vs. Cu; (H) Ag+Cu vs. In; (I) Ga+Ge+As+Sb vs. Ag+Cu.

and low-temperature sphalerite usually contains > 50 ppm Ge (Cugerone et al., 2018; Wei et al., 2021). In this study, Ge contents in sphalerite range from 0.30 to 50.2 ppm, predominantly falling within the medium-temperature range. The In/Ge ratios vary from 0.002 to 545 (average 67.4), which are elevated relative to low-temperature deposits but notably lower than those reported for high-temperature deposits (e.g., Goutouling mine in Furong tin ore field, In/Ge = 2091–16923; Ye et al., 2012). Ga/In ratios primarily range from 0.26 to 60, with occasional values exceeding 100, consistent with low- to medium-temperature sphalerite.

Trace-element thermometers for sphalerite provide a quantitative tool for estimating its mineralization temperature. Keith et al. (2014) proposed a geothermometer based on the Fe and Zn contents of sphalerite (Equation 1), which yields crystallization temperatures of 233 °C–276 °C (mean = 257 °C) for the Luobugaizi deposit. Temperature calculation using the GGIMF thermometer (Frenzel et al., 2016) yields a range from 140 °C to 283 °C, with a mean of 195 °C.

$$\text{Fe/Zn}_{\text{sphalerite}} = 0.0013(T) - 0.2953 \quad (1)$$

Recently, machine learning approaches have been applied to trace element data for sphalerite geothermometry. Meng et al. (2024), Zhao et al. (2024) developed a Sphalerite Random Forest Thermometer (SPRFT) software. Applying this software to Luobugaizi trace element data yields temperatures of 135 °C–279 °C, with a mean of 220 °C ± 26 °C. All the calculated temperatures are listed in the Supplementary Material.

The average values calculated by three different methods for the formation temperature of sphalerite range from 195 °C to 257 °C, indicating a low- to medium-temperature mineralization condition for Luobugaizi.

## 5.3 Source of ore-forming materials

### 5.3.1 Source of sulfur

Multiple studies have demonstrated that the S isotopic composition of sulfides is a key tracer for determining sulfur sources, offering deeper insights into deposit formation (Bachinski, 1969; Gao et al., 2020b; Meng et al., 2022; Cheng et al., 2024; Liu et al., 2024; Duan et al., 2025). Distinct geological reservoirs possess characteristic  $\delta^{34}\text{S}$  signatures. For instance, magmatic sulfur typically ranges within 0‰ ± 3‰, Silurian seawater sulfate varies between +21‰ and +36‰, while metamorphic ( $\delta^{34}\text{S} = -20‰$  to +20‰) and sedimentary sulfur ( $\delta^{34}\text{S} = -40‰$  to +40‰) exhibit much broader ranges (Ohmoto, 1979; Claypool et al., 1980; Chaussidon and Lorand, 1990; Kampschulte and Strauss, 2004; Zhou J. X. et al., 2013; Rodiouchkina et al., 2023).

The  $\delta^{34}\text{S}$  values of sphalerite from the Luobugaizi deposit range from -1.2‰ to +3.3‰, similar to previous study ( $\delta^{34}\text{S} = -6‰$ –+6‰, Jiang et al., 2024). This limited range, coupled with a unimodal frequency distribution (Figure 6), suggests derivation from a relatively homogeneous sulfur source. Under the reducing conditions indicated by the simple sulfide assemblage (sphalerite, galena, pyrite ± chalcopyrite, with no sulfate minerals detected), the average  $\delta^{34}\text{S}$  value of sphalerite (+1.3‰) can approximately represent the sulfur isotope composition of the ore-forming fluid (Ohmoto, 1972).

The  $\delta^{34}\text{S}$  signature of Luobugaizi closely resembles those of Laihesan (-2‰ to +6‰) and Sachakou (-6‰ to +4‰) from the same ore belt (Figure 8), both previously interpreted as magmatic-hydrothermal in origin (Jiang et al., 2024). This cluster contrasts sharply with other genetic types in the region: Mississippi Valley-type (MVT) deposits (e.g., Duobaoshan, Du et al., 2012; Kalayashake; Yu et al., 2013) generally show more negative values, whereas sediment-involved or stratified systems (e.g., Huoshaoyun, Ren et al., 2024; Caixiashan; Gao et al., 2007) exhibit markedly wider ranges (Figure 8). The consistently near-zero, tightly clustered  $\delta^{34}\text{S}$  values at Luobugaizi are thus inconsistent with dominant sulfur derivation from sedimentary or basinal brine sources, but instead align with a deep-sourced magmatic reservoir.

### 5.3.2 Source of lead

Pb isotopes remain relatively stable during mineral transport and precipitation due to minimal fractionation (Tera, 2006; Zhou et al., 2014; Li et al., 2023). In tracing mineralizing substances in diverse ore deposits, Pb isotopes serve as highly effective and direct approaches (Zartman and Doe, 1981; Ehya et al., 2010; Pass et al., 2014; Rddad and Bouhleb, 2016; Liebmann et al., 2024). The Pb isotopic composition of the Luobugaizi shows a narrow variation and relatively homogeneous ratios. The Pb isotopic compositions of sulfides from the Luobugaizi deposit are similar to the compositions of sulfides from other Pb-Zn deposits within West Kunlun Qiao'er-Tianshan region, including the Huoshaoyun (217–216 Ma, Li et al., 2019; Ren et al., 2024) and Honghuangling deposit (159 ± 1.4 Ma, Zhang et al., 2018; Zhang J. K. et al., 2022), but significantly differ from those of the Xinjiang Caixiashan - (351.9 ± 3.5 Ma, Gao et al., 2007; Gao et al., 2020 R. Z.) and Duobaoshan deposits (195 ± 1.1 Ma, Du et al., 2012; Zhou et al., 2019). As the host rock of the Luobugaizi deposit, the Silurian Wenquanguo Formation sedimentary rocks may provide Pb and Zn for the mineralization. However, previous study have shown that the Wenquanguo Formation has low Pb and Zn concentrations, which are insufficient to serve as the main Pb-Zn source or achieve metallogenic enrichment (Zhao et al., 2014).

To further investigate the origin of Pb in the Luobugaizi Pb-Zn deposit, the Pb isotopic composition of the ore was analyzed using a Pb tectonic environment model. In the  $^{207}\text{Pb}/^{204}\text{Pb}$ - $^{206}\text{Pb}/^{204}\text{Pb}$  diagram (Figure 9A), sulfides mainly plot within the lower crustal Pb source field; in the  $^{208}\text{Pb}/^{204}\text{Pb}$ - $^{206}\text{Pb}/^{204}\text{Pb}$  diagram (Figure 9B), they fall within the overlap of the lower crustal and orogenic belt fields. Moreover, the regional Cretaceous granitoids show similar Pb isotopic ratios, with average  $^{206}\text{Pb}/^{204}\text{Pb} = 18.44$ ,  $^{207}\text{Pb}/^{204}\text{Pb} = 15.72$ ,  $^{208}\text{Pb}/^{204}\text{Pb} = 38.78$  (Yang F. et al., 2024).

Previous studies indicate that the Cretaceous granitoids (e.g., Kalaqigu granite) in this region, emplaced at 107–102 Ma, were generated by partial melting of Precambrian lower crust with variable involvement of mafic magma (Liu et al., 2020a). The Pb tectonic model also suggests that Pb was mainly derived from lower crust. Therefore, the Luobugaizi Pb-Zn deposit has the same Pb source with the regional granitoids. The mineralization age of the deposit (ca. 99 Ma, Wang et al., 2021) closely follows the emplacement of these granitoids, indicating a temporal and genetic link between magmatism and mineralization. The ore-forming materials were likely supplied by hydrothermal fluids differentiated from the Cretaceous magma.

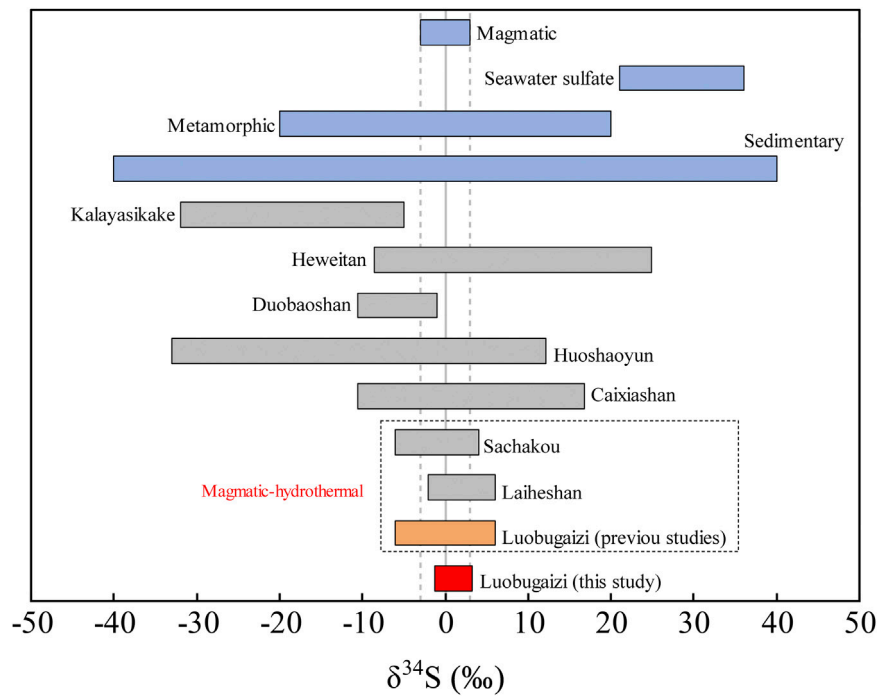


**FIGURE 8**  
Comparison of S isotopes of Luobugaizi with different reservoirs and different deposits.

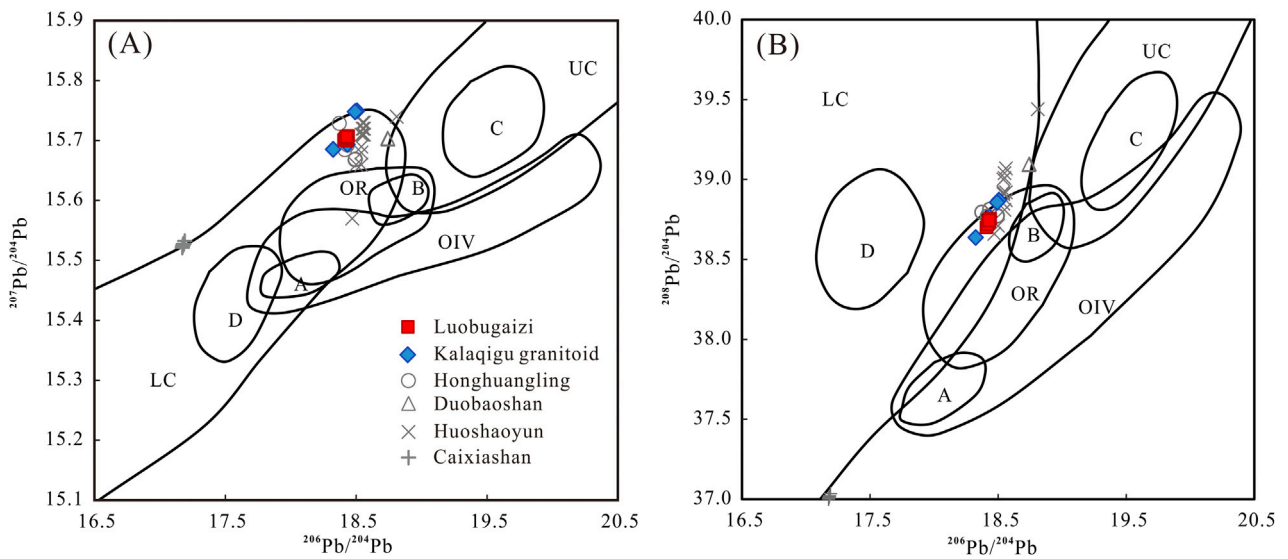
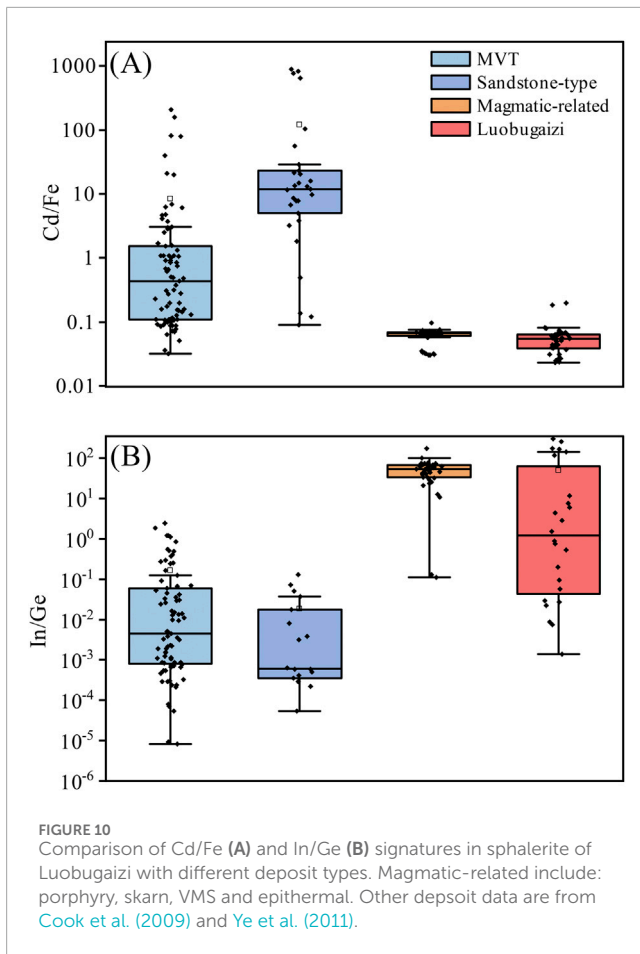


**FIGURE 9**  
 $^{206}\text{Pb}/^{204}\text{Pb}$ - $^{207}\text{Pb}/^{204}\text{Pb}$  (A) and  $^{206}\text{Pb}/^{204}\text{Pb}$ - $^{208}\text{Pb}/^{204}\text{Pb}$  (B) discriminant diagram of Luobugaizi Pb-Zn deposit (modified after Zartman and Doe, 1981). LC-Lower Crust; UC-Upper Crust; OIV-Oceanic Island Volcanics; OR-Orogenic belt. A, B, C, and D represent the probable average values of mantle, orogen, upper crust and lower crust. Data for the Kalaqigu granitoid are from Yang et al. (2024a), Data for the Duobaoshan deposit are from Du et al. (2012), Data for the Huoshaoyun deposit are from Ren et al. (2024), Data for the Caixiashan deposit are from Gao et al. (2007) and for the Honghuangling deposit are from Zhang et al. (2018).

### 5.4 Genesis of the Luobugaizi deposit

The mineralization of Luobugaizi Pb-Zn deposit is characterized by an assemblage of sphalerite, galena, pyrite, and minor

chalcopyrite, accompanied by hydrothermal alteration such as silicification, sericitization, and chloritization. Together, this mineral assemblage and alteration features indicate a low-to medium-temperature hydrothermal origin for the deposit.



Trace element contents and ratios in sulfides of Pb-Zn deposits can indirectly indicate the deposit's genetic type (Cook et al., 2009; Belissant et al., 2014; Yuan B. et al., 2018). For instance, in magmatic-hydrothermal deposits, the Cd/Fe ratio is generally stable and below 0.1, In/Ge ratio typically exceeds 0.1, commonly approaching

50. MVT deposits show considerable variation of Cd/Fe ratios ranging from 0.08 to 10, with In/Ge typically less than 0.1, while sandstone-hosted deposits exhibit the widest Cd/Fe ratio range of 0.15–100, In/Ge less than 0.03 (Cook et al., 2009; Ye et al., 2011; Gao et al., 2024). At Luobugaizi, sphalerite yields Cd/Fe ratios of 0.02–0.08 (mean 0.03) (Figure 10A) and In/Ge predominantly exceeds 0.1 (mean 50.1) (Figure 10B), indicating a clear genetic link to magmatic activity.

Isotope geochemistry further supports this interpretation. Both the  $\delta^{34}\text{S}$  values (showing a narrow, near-zero, and tower-shaped distribution) and the Pb isotopic composition (similar to Cretaceous granites) suggest a common origin from a magmatic-related hydrothermal fluid.

The Luobugaizi deposit exhibits a close spatial and temporal association with Late Yanshanian magmatism. In the southern part of the deposit, there are outcrops of Late Yanshanian biotite granite (Figure 1B) and to the east, Late Yanshanian monzonitic granite aligns along the Qunsaragiriya Fault (F5). The granite exposed to the east of the deposit has yielded a weighted mean age of 107–102 Ma (Liu et al., 2020a). Wang et al. (2021) obtained a monazite U-Pb age of ca. 99 Ma from light-colored veins closely related to Pb-Zn mineralization, which they interpreted as the mineralization age of the Luobugaizi deposit. This mineralization age overlaps, within analytical uncertainty, with the emplacement age of the granite, underscoring their temporal connection.

Previous studies on regional plate tectonic evolution indicate that during the Early Cretaceous, the Neo-Tethyan oceanic lithosphere likely underwent low-angle to flat subduction beneath South Pamir-Karakoram (Liu et al., 2020a; Zhang C. L. et al., 2022; Yang F. et al., 2024). Consequently, a series of granitoids were interpreted in previous studies as products of partial melting of the Precambrian lower crust with mantle-derived inputs during ca. 107–102 Ma (Liu et al., 2020a; Yang F. et al., 2024). Subsequent differentiation and fluid exsolution from this crust-mantle interaction derived magmas provided a potential source for the ore-forming materials (Figure 11).

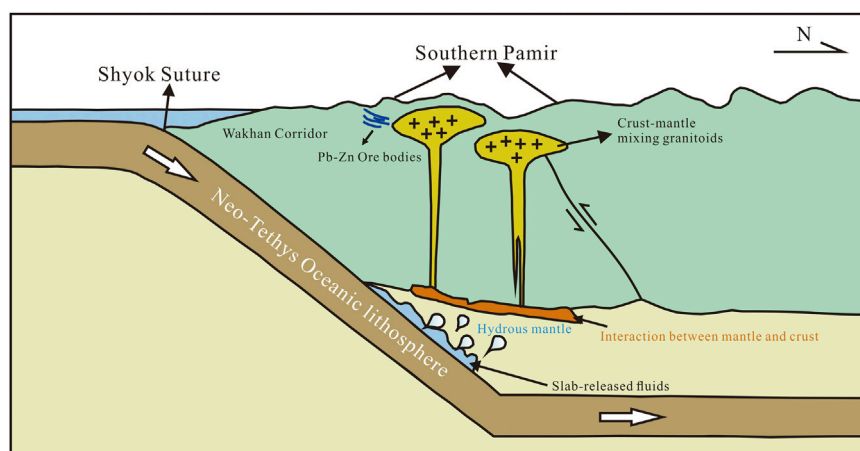


**FIGURE 11**  
A cartoon illustrating the genesis and geodynamic setting of Luobugaizi Pb-Zn deposit. Northward low-angle subduction of the Neo-Tethyan oceanic lithosphere resulted in the generation of Cretaceous granitoids and related Luobugaizi Pb-Zn deposit (modified after Yang F. et al., 2024).

The host rock of Luobugaizi deposit is dominated by relatively soft and deformable slate. Regional tectonic deformation induced tensile fracturing within these rocks, creating pathways for hydrothermal Pb-Zn-bearing fluids to migrate along faults and fractures and ultimately precipitate ore minerals within the host sequence.

In conclusion, the mineralogical, geochemical, and geological characteristics of Luobugaizi Pb-Zn deposit are consistent with a magmatic-hydrothermal origin.

## 6 Conclusion

The large Luobugaizi Pb-Zn deposit is in the northwestern part of the West Kunlun-Karakoram Pb-Zn ore belt. The ores are hosted in Silurian clastic rocks, with sphalerite, galena and pyrite as main ore minerals. This mineral assemblage and sphalerite trace element geothermometers indicate the Luobugaizi Pb-Zn deposit formed mainly at a low to medium temperature. Sulfur isotopes ( $\delta^{34}\text{S} = -1.2$  to  $+3.3\text{‰}$ ) and narrow Pb isotopic ranges indicate a homogeneous, deep-sourced magmatic fluid.

Based on its geological and mineralization features, trace elements and isotopic compositions, the Luobugaizi Pb-Zn deposit is genetically linked to Cretaceous magmatic-hydrothermal activity which might be triggered by Neo-Tethyan oceanic subduction. The deposit is classified as a low-to medium-temperature magmatic-hydrothermal type.

## Data availability statement

The original contributions presented in the study are included in the article/[Supplementary Material](#), further inquiries can be directed to the corresponding author.

## Author contributions

R-HH: Methodology, Writing – original draft. H-XZ: Investigation, Writing – review and editing. J-XW: Investigation, Writing – review and editing. C-LZ: Writing – review and editing, Investigation.

## References

- Ault, K. M. (2004). Sulfur and lead isotope study of the El mochito zn-pb-ag deposit. *Econ. Geol.* 99 (6), 1223–1231. doi:10.2113/99.6.1223
- Babedi, L., Von Der Heyden, B. P., Neethling, P. H., and Tadie, M. (2019). The effect of Cd-substitution on the Raman vibrational characteristics of sphalerite. *Vib. Spectrosc.* 105, 102968. doi:10.1016/j.vibspec.2019.102968
- Bachinski, D. J. (1969). Bond strength and sulfur isotopic fractionation in coexisting sulfides. *Econ. Geol.* 64 (1), 56–65. doi:10.2113/gsecongeo.64.1.56
- Bao, Z. A., Chen, L., Zong, C. L., Yuan, H. L., Chen, K. Y., and Dai, M. N. (2017). Development of pressed sulfide powder tablets for *in situ* sulfur and lead isotope measurement using LA-MC-ICP-MS. *Int. J. Mass Spectrom.* 421, 255–262. doi:10.1016/j.ijms.2017.07.015
- Bauer, M. E., Burisch, M., Ostendorf, J., Krause, J., Frenzel, M., Seifert, T., et al. (2019a). Trace element geochemistry of sphalerite in contrasting hydrothermal

## Funding

The author(s) declared that financial support was received for this work and/or its publication. This research was supported by projects from the National Natural Science Foundation of China (NSFC No. 42172062).

## Conflict of interest

Author J-XW was employed by Chengdu Xinli Geological Exploration Co., Ltd.

The remaining author(s) declared that this work was conducted in the absence of any commercial or financial relationships that could be construed as a potential conflict of interest.

## Generative AI statement

The author(s) declared that generative AI was not used in the creation of this manuscript.

Any alternative text (alt text) provided alongside figures in this article has been generated by Frontiers with the support of artificial intelligence and reasonable efforts have been made to ensure accuracy, including review by the authors wherever possible. If you identify any issues, please contact us.

## Publisher's note

All claims expressed in this article are solely those of the authors and do not necessarily represent those of their affiliated organizations, or those of the publisher, the editors and the reviewers. Any product that may be evaluated in this article, or claim that may be made by its manufacturer, is not guaranteed or endorsed by the publisher.

## Supplementary material

The Supplementary Material for this article can be found online at: <https://www.frontiersin.org/articles/10.3389/feart.2025.1736494/full#supplementary-material>

fluid systems of the freiberg district, Germany: insights from LA-ICP-MS analysis, near-infrared light microthermometry of sphalerite-hosted fluid inclusions, and sulfur isotope geochemistry. *Min. Deposita* 54, 237–262. doi:10.1007/s00126-018-0850-0

Bauer, M. E., Seifert, T., Burisch, M., Krause, J., Richter, N., and Gutzmer, J. (2019b). Indium-bearing sulfides from the Hämmerlein skarn deposit, Erzgebirge, Germany: evidence for late-stage diffusion of indium into sphalerite. *Min. Deposita* 54, 175–192. doi:10.1007/s00126-017-0773-1

Belissant, R., Boiron, M. C., Luais, B., and Cathelineau, M. (2014). LA-ICP-MS analyses of minor and trace elements and bulk Ge isotopes in zoned Ge-rich sphalerites from the Noailhac-saint-salvy deposit (France): insights into incorporation mechanisms and ore deposition processes. *Geochim. Cosmochim. Acta* 126, 518–540. doi:10.1016/j.gca.2013.10.052

- Belissant, R., Munoz, M., Boiron, M. C., Luais, B., and Mathon, O. (2016). Distribution and oxidation state of Ge, Cu and Fe in sphalerite by  $\mu$ -XRF and K-edge  $\mu$ -XANES: insights into Ge incorporation, partitioning and isotopic fractionation. *Geochim. Cosmochim. Acta* 177, 298–314. doi:10.1016/j.gca.2016.01.001
- Benedetto, R. D., Bernardini, G. P., Costagliola, P., Plant, D., and Vaughan, D. J. (2005). Compositional zoning in sphalerite crystals. *Am. Mineral.* 90 (8-9), 1384–1392. doi:10.2138/am.2005.1754
- Bonnet, J., Mosser-Ruck, R., Caumon, M. C., Rouer, O., Andre-Mayer, A. S., Cauzid, J., et al. (2016). Trace element distribution (Cu, Ga, Ge, Cd, and Fe) in sphalerite from the Tennessee MVT deposits, USA, by combined EMPA, LA-ICP-MS, Raman spectroscopy, and crystallography. *Can. Mineral.* 54 (5), 1261–1284. doi:10.3749/canmin.1500104
- Chaussidon, M., and Lorand, J. P. (1990). Sulphur isotope composition of orogenic spinel Iherzolite massifs from Ariège (North-Eastern Pyrenees, France): an ion microprobe study. *Geochim. Cosmochim. Acta* 54 (10), 2835–2846. doi:10.1016/0016-7037(90)90018-g
- Chen, L., Chen, K. Y., Bao, Z. A., Liang, P., Sun, T. T., and Yuan, H. L. (2017). Preparation of standards for *in situ* sulfur isotope measurement in sulfides using femtosecond laser ablation MC-ICP-MS. *J. Anal. At. Spectrom.* 32 (1), 107–116. doi:10.1039/c6ja00270f
- Cheng, X. L., Zhou, Y. M., Wang, J. Y., Zhao, C. F., Huang, J., Li, P. J., et al. (2024). Sources and ore-forming environment of the Jinchanghe Pb-Zn polymetallic skarn deposit, baoshan block, SW China: constraints from Cu-S isotopic and trace elemental compositions of sulfides. *Minerals* 14 (7), 644. doi:10.3390/min14070644
- Ciobanu, C. L., Cook, N. J., Utsunomiya, S., Kogagwa, M., Green, L., Gilbert, S., et al. (2012). Gold-telluride nanoparticles revealed in arsenic-free pyrite. *Am. Mineral.* 97 (8-9), 1515–1518. doi:10.2138/am.2012.4207
- Claypool, G. E., Holsler, W. T., Kaplan, I. R., Sakai, H., and Zak, I. (1980). The age curves of sulfur and oxygen isotopes in marine sulfate and their mutual interpretation. *Chem. Geol.* 28, 199–260. doi:10.1016/0009-2541(80)90047-9
- Cook, N. J., Ciobanu, C. L., Pring, A., Skinner, W., Shimizu, M., Danyushevsky, L., et al. (2009). Trace and minor elements in sphalerite: a LA-ICP-MS study. *Geochim. Cosmochim. Acta* 73 (16), 4761–4791. doi:10.1016/j.gca.2009.05.045
- Cook, N. J., Ciobanu, C. L., and Williams, T. (2011). The mineralogy and mineral chemistry of indium in sulphide deposits and implications for mineral processing. *Hydrometallurgy* 108 (3-4), 226–228. doi:10.1016/j.hydromet.2011.04.003
- Cook, N. J., Ciobanu, C. L., Brugger, J., Etschmann, B., Howard, D. L., de Jonge, M. D., et al. (2012). Determination of the oxidation state of Cu in substituted Cu-In-Fe-bearing sphalerite via  $\mu$ -XANES spectroscopy. *Am. Mineral.* 97 (2-3), 476–479. doi:10.2138/am.2012.4042
- Cugerone, A., Cenko-Tok, B., Chauvet, A., Le Goff, E., Bailly, L., Alard, O., et al. (2018). Relationships between the occurrence of accessory Ge-minerals and sphalerite in variscan Pb-Zn deposits of the bossois anticlinorium, French pyrenean axial zone: chemistry, microstructures and ore-deposit setting. *Ore Geol. Rev.* 95, 1–19. doi:10.1016/j.oregeorev.2018.02.016
- Ding, T., Ma, D. S., Lu, J. J., Zhang, R. Q., and Zhang, S. T. (2016). S, Pb, and Sr isotope geochemistry and genesis of Pb-Zn mineralization in the huangshaping polymetallic ore deposit of southern Hunan Province, China. *Ore Geol. Rev.* 77, 117–132. doi:10.1016/j.oregeorev.2016.02.010
- Dong, Y. G., Guo, K. Y., Liao, S. B., Xiao, H. I., and Wang, T. (2006). Geological and geochemical characteristics of the kekuxilik lead-zinc ore deposit, West Kunlun, Xinjiang. *Acta Geol. Sin.* 80 (11), 1730–1738. (in Chinese with English abstract).
- Du, H. X., Wei, Y. F., Xue, C. J., Qi, T. J., Jin, H. Z., Lin, M. Y., et al. (2012). Geological and geochemical characteristics of duobaoshan Pb-Zn deposit in Hetian, Xinjiang. *Xinjiang Geol.* 30 (01), 52–57. (in Chinese with English abstract).
- Duan, M. X., Chen, G. H., Liu, T., Liu, L. Y., and Zhao, X. D. (2025). Analysis of metallogenic material sources and metallogenic epoch of the xiahulun lead-zinc deposit in inner Mongolia, China. *Front. Earth Sci.* 13, 1536511. doi:10.3389/feart.2025.1536511
- Ehya, F., Lotfi, M., and Rasa, I. (2010). Emarat carbonate-hosted Zn-Pb deposit, Markazi Province, Iran: a geological, mineralogical and isotopic (S, Pb) study. *J. Asian Earth Sci.* 37 (2), 186–194. doi:10.1016/j.jseas.2009.08.007
- Faisal, M., Yang, X. Y., Zhang, H. S., Amuda, A. K., Sun, C., Mustafa, S., et al. (2022). Mineralization styles, alteration mineralogy, and sulfur isotope geochemistry of volcanogenic massive sulfide deposits in the shadli metovolcanics belt, South Eastern Desert, Egypt: metallogenic implications. *Ore Geol. Rev.* 140, 104402. doi:10.1016/j.oregeorev.2021.104402
- Frenzel, M., Hirsch, T., and Gutzmer, J. (2016). Gallium, germanium, indium, and other trace and minor elements in sphalerite as a function of deposit type—A meta-analysis. *Ore Geol. Rev.* 76, 52–78. doi:10.1016/j.oregeorev.2015.12.017
- Frenzel, M., Voudouris, P., Cook, N. J., Ciobanu, C. L., Gilbert, S., and Wade, B. P. (2022). Evolution of a hydrothermal ore-forming system recorded by sulfide mineral chemistry: a case study from the plaka Pb-Zn-Ag deposit, Lavrion, Greece. *Min. Deposita* 57, 1–22. doi:10.1007/s00126-021-01067-y
- Gao, J. G., Liang, T., Peng, M. X., Li, Y. L., Wang, L., and Gao, X. L. (2007). Sulfur, carbon, hydrogen and oxygen isotope geochemistry of caixishan lead-zinc deposit, Xinjiang. *Geol. Explor.* (05), 57–60. (in Chinese with English abstract).
- Gao, R. Z., Xue, C. J., Chi, G. X., Dai, J. F., Dong, C., Zhao, X. B., et al. (2020a). Genesis of the giant caixishan Zn-Pb deposit in Eastern Tianshan, NW China: constraints from geology, geochronology and S-Pb isotopic geochemistry. *Ore Geol. Rev.* 119, 103366. doi:10.1016/j.oregeorev.2020.103366
- Gao, F., Jian, K. K., Zhang, Z. K., Pan, L., and Du, B. (2020b). Geological characteristics and genesis analysis of baozishan Pb-Zn deposit in Karakoram Area. *Northwest. Geol.* 53 (02), 172–182. (in Chinese with English abstract). doi:10.19751/j.cnki.61-1149/p.2020.02.010
- Gao, X., Zhou, Z. H., Breiter, K., Mao, J. W., Romer, R. L., Cook, N. J., et al. (2024). Magmatic-hydrothermal fluid evolution of the tin-polymetallic metallogenic systems from the Weilasituo ore district, Northeast China. *Sci. Rep.* 14 (1), 3006. doi:10.1038/s41598-024-53579-y
- George, L., Cook, N. J., and Wade, B. P. (2015). Trace and minor elements in galena: a reconnaissance LA-ICP-MS study. *Am. Mineral.* 100 (2-3), 548–569. doi:10.2138/am-2015-4862
- Gill, S. B., Piercey, S. J., Layne, G. D., and Piercey, G. (2019). Sulphur and lead isotope geochemistry of sulphide minerals from the Zn-Pb-Cu-Ag-Au lemarchant volcanogenic massive sulfide (VMS) deposit, Newfoundland, Canada. *Ore Geol. Rev.* 104, 422–435. doi:10.1016/j.oregeorev.2018.11.008
- Hong, T., Harlaux, M., Zhai, M. G., Wang, Y. J., Xu, X. W., Xia, X. P., et al. (2025). Syn-tectonic emplacement of Li-bearing pegmatites related to detachment faulting in the dahongliutan pegmatite belt. *Min. Deposita*. doi:10.1007/s00126-025-01352-0
- Hu, Y. S., Wei, C., Ye, L., Huang, Z. L., Danyushevsky, L., and Wang, H. Y. (2021). LA-ICP-MS sphalerite and galena trace element chemistry and mineralization-style fingerprinting for carbonate-hosted Pb-Zn deposits: perspective from early Devonian huodehong deposit in Yunnan, South China. *Ore Geol. Rev.* 136, 104253. doi:10.1016/j.oregeorev.2021.104253
- Jiang, G. P., Li, H., Tian, Y., and Zhang, L. (2024). Metallogenic model and ore-controlling factors of lead-zinc deposits in the Qiao'er-Tianshan area of western Kunlun Mountains. *J. Geol.* 48 (01), 1–8. (in Chinese with English abstract).
- Kampschulte, A., and Strauss, H. (2004). The sulfur isotopic evolution of Phanerozoic seawater based on the analysis of structurally substituted sulfate in carbonates. *Chem. Geol.* 204 (3-4), 255–286. doi:10.1016/j.chemgeo.2003.11.013
- Keith, M., Haase, K. M., Schwarz-Schampera, U., Klemm, R., Petersen, S., and Bach, W. (2014). Effects of temperature, sulfur, and oxygen fugacity on the composition of sphalerite from submarine hydrothermal vents. *Geology* 42 (8), 699–702. doi:10.1130/G35655.1
- Li, H., Xu, X. W., Borg, G., Gilg, H. A., Dong, L. H., Fan, T. B., et al. (2019). Geology and geochemistry of the giant huoshaoyun zinc-lead deposit, Karakoram Range, northwestern Tibet. *Ore Geol. Rev.* 106, 251–272. doi:10.1016/j.oregeorev.2019.02.002
- Li, Z. L., Ye, L., Hu, Y. S., Wei, C., Huang, Z. L., Yang, Y. L., et al. (2020). Trace elements in sulfides from the Maozu Pb-Zn deposit, Yunnan Province, China: implications for trace-element incorporation mechanisms and ore genesis. *Am. Mineral.* 105 (11), 1734–1751. doi:10.2138/am-2020-6950
- Li, L. J., Han, R. S., Zhang, Y., Wu, J. B., and Feng, Z. X. (2022). Trace element signatures of sphalerite in the Sichuan Daliangzi Ge-rich Pb-Zn deposit and its implications for deep ore prospecting. *Front. Earth Sci.* 10, 928738. doi:10.3389/feart.2022.928738
- Li, S. H., Li, Z. X., Chen, G. Z., Yi, H. N., Yang, F., Lü, X., et al. (2023). Age, fluid inclusion, and h-o-s-pb isotope geochemistry of the superlarge Huaobaote ag-pb-zn deposit in the Southern great Xing'an Range, NE China. *Minerals* 13 (7), 939. doi:10.3390/min13070939
- Li, Z., Lang, X. H., Liu, H., Zhan, H. Y., Tan, H., and Zhang, P. (2024). Trace element composition characteristics of sphalerite in the Pusanguo Co-Cu-Pb-Zn deposit in Tibet and its indicative significance. *Acta Geol. Sin.* 98 (10), 3077–3097. (in Chinese with English abstract). doi:10.19762/j.cnki.dizhixuebao.2023373
- Liebmann, J., Ware, B., Mole, D. R., Kirkland, C. L., Fraser, G., Waltenberg, K., et al. (2024). A crustal Pb isotope map of southeastern Australia. *Sci. Data* 11 (1), 1222. doi:10.1038/s41597-024-03996-5
- Liu, X. Q., Zhang, C. L., Hao, X. S., Zou, H. B., Zhao, H. X., and Ye, X. T. (2020a). Early Cretaceous granitoids in the Southern Pamir: implications for the Mesozoic evolution of the Pamir plateau. *Lithos* 362, 105492. doi:10.1016/j.lithos.2020.105492
- Liu, X. Q., Zhang, C. L., Zou, H., Wang, Q., Hao, X. S., Zhao, H. X., et al. (2020b). Triassic-Jurassic granitoids and pegmatites from Western Kunlun-Pamir syntax: implications for the paleo-tethys evolution at the northern margin of the Tibetan Plateau. *Lithosphere* 1, 7282037. doi:10.2113/2020/7282037
- Liu, H., Dong, S. Y., Liu, Y. L., Lin, X. Y., Liu, Y. H., Wang, H., et al. (2024). Ore-forming material sources of the Pakbeng gold deposit, Laos: evidence from fluid inclusions, HOS isotopes, and trace elements. *Ore Energy Resour. Geol.* 17, 100047. doi:10.1016/j.oreoa.2024.100047
- Liu, Y. H., Han, R. S., Zhang, Y., Chen, Y., and Wu, J. B. (2025). Coloration mechanism of Fe in sphalerite based on LA-ICP-MS and DFT: a case study of the huize super-large Ge-rich Ag-Pb-Zn deposit in Sichuan-Yunnan-Guizhou. *Ore Geol. Rev.* 180, 106550. doi:10.1016/j.oregeorev.2025.106550

- Lockington, J. A., Cook, N. J., and Ciobanu, C. L. (2014). Trace and minor elements in sphalerite from metamorphosed sulphide deposits. *Minerl. Petrol.* 108, 873–890. doi:10.1007/s00710-014-0346-2
- Luo, K., Cugerone, A., Zhou, M. F., Zhou, J. X., Sun, G. T., Xu, J., et al. (2022). Germanium enrichment in sphalerite with acicular and euhedral textures: an example from the zhulingou carbonate-hosted Zn (-Ge) deposit, south China. *Min. Deposita* 57 (8), 1343–1365. doi:10.1007/s00126-022-01112-4
- Makovicky, E., and Topa, D. (2015). Crystal chemical formula for sartorite homologues. *Mineral. Mag.* 79 (1), 25–31. doi:10.1180/minmag.2015.079.1.03
- Mason, P. R., Košler, J., de Hoog, J. C., Sylvester, P. J., and Meffan-Main, S. (2006). *In situ* determination of sulfur isotopes in sulfur-rich materials by laser ablation multiple-collector inductively coupled plasma mass spectrometry (LA-MC-ICP-MS). *J. Anal. At. Spectrom.* 21 (2), 177–186. doi:10.1039/b510883g
- Meng, Y. M., Huang, X. W., Xu, C. X., and Meng, S. N. (2022). Trace element and sulfur isotope compositions of pyrite from the tianqiao Zn–Pb–Ag deposit in Guizhou province, SW China: implication for the origin of ore-forming fluids. *Acta Geochim.* 41, 1–18. doi:10.1007/s11631-021-00511-0
- Meng, Y. M., Huang, X. W., Hu, R. Z., Beaudoin, G., Zhou, M. F., and Meng, S. N. (2024). Deposit type discrimination based on trace elements in sphalerite. *Ore Geol. Rev.* 165, 105887. doi:10.1016/j.oregeorev.2024.105887
- Möller, P. (1985). Development and application of the Ga/Ge-geothermometer for sphalerite from sediment-hosted deposits. *Monogr. Ser. Min. Deposits* 25, 15–30.
- Ohmoto, H. (1972). Systematics of sulfur and carbon isotopes in hydrothermal ore deposits. *Econ. Geol.* 67 (5), 551–578. doi:10.2113/gsecongeo.67.5.551
- Ohmoto, H. (1979). “Isotope of sulfur and carbon,” in *Geochemistry of hydrothermal ore deposits*, 509–567.
- Pass, H. E., Cooke, D. R., Davidson, G., Maas, R., Dipple, G., Rees, C., et al. (2014). Isotope geochemistry of the Northeast zone, Mount Polley alkalic Cu–Au–Ag porphyry deposit, British Columbia: a case for carbonate assimilation. *Econ. Geol.* 109 (4), 859–890. doi:10.2113/econgeo.109.4.859
- Pfaff, K., Wagner, T., and Markl, G. (2009). Fluid mixing recorded by mineral assemblage and Mineral chemistry in a Mississippi Valley-Type Pb–Zn–Ag deposit in Wiesloch, SW Germany. *J. Geochem. Explor.* 101 (1), 81. doi:10.1016/j.gexplo.2008.12.022
- Qiao, G. B., Wang, P., Wu, Y. Z., Hao, Y. H., Zhao, X. J., Chen, D. H., et al. (2015). Formation age of ore-bearing strata of the Zankan iron deposit in taxkorgan landmass of Western Kunlun Mountains and its geological significance. *Geol. China* 42 (03), 616–629. doi:10.3969/j.issn.1000-3657.2015.03.016 (in Chinese with English abstract).
- Qiao, G. B., Wu, Y. Z., and Liu, T. (2021). Zircon U–Pb age of pegmatite veins in Dahongliutan lithium deposit, western Kunlun. *China Geol.* 4 (1), 185–187. doi:10.31035/CG2020061
- Quek, L. X. (2018). *Early to middle Paleozoic volcanism of Western peninsular Malaysia*. Malaysia: University of Malaya. [dissertation's thesis].
- Rddad, L., and Bouhleh, S. (2016). The bou dahar Jurassic carbonate-hosted Pb–Zn–Ba deposits (Oriental High Atlas, Morocco): Fluid-inclusion and C–O–S–Pb isotope studies. *Ore Geol. Rev.* 72, 1072–1087. doi:10.1016/j.oregeorev.2015.08.011
- Reich, M., Deditius, A., Chrysosulis, S., Li, J. W., Ma, C. Q., Parada, M. A., et al. (2013). Pyrite as a record of hydrothermal fluid evolution in a porphyry copper system: a SIMS/EMPA trace element study. *Geochim. Cosmochim. Acta* 104, 42–62. doi:10.1016/j.gca.2012.11.006
- Ren, G. L., Huang, C. Y., Yang, M., Yao, A. Q., Zhao, X. J., Zhang, H. S., et al. (2024). Geochemical characteristics and geological significance of the huoshaoyun lead-zinc deposit, Xinjiang. *Geotecton. Metallog.* 48 (03), 654–675. (in Chinese with English abstract). doi:10.16539/j.ddgzyckx.2024.03.016
- Rodiouchkina, K., Rodushkin, I., Goderis, S., and Vanhaecke, F. (2023). A comprehensive evaluation of sulfur isotopic analysis ( $\delta^{34}\text{S}$  and  $\delta^{33}\text{S}$ ) using multi-collector ICP-MS with characterization of reference materials of geological and biological origin. *Anal. Chim. Acta* 1240, 340744. doi:10.1016/j.aca.2022.340744
- Shen, P., Shen, Y. C., Liu, T. B., Li, G. M., and Zeng, Q. D. (2007). Genesis of volcanic-hosted gold deposits in the Sawur gold belt, northern Xinjiang, China: evidence from REE, stable isotopes, and noble gas isotopes. *Ore Geol. Rev.* 32 (1–2), 207–226. doi:10.1016/j.oregeorev.2006.10.005
- Sun, B. K., Lv, X. B., Wang, S. G., Ulrich, T., Dai, Z. H., and Ruan, B. X. (2023). Evolution of an ancient VMS ore-forming system recorded by pyrite and sphalerite mineral texture, trace elements, and sulfur isotope: a case study from the Huangtupo Cu–Zn (-Au) deposit, Eastern Tianshan, NW China. *Ore Geol. Rev.* 158, 105475. doi:10.1016/j.oregeorev.2023.105475
- Tera, F. (2006). Lead isotope planetary profiling (LIPP): summation–depiction of Earth's many reservoirs. *Chem. Geol.* 233 (1–2), 1–45. doi:10.1016/j.chemgeo.2006.02.007
- Torró, L., Benites, D., Vallance, J., Laurent, O., Ortiz-Benavente, B. A., Chelle-Michou, C., et al. (2022). Trace element geochemistry of sphalerite and chalcopyrite in arc-hosted VMS deposits. *J. Geochem. Explor.* 232, 106882. doi:10.1016/j.gexplo.2021.106882
- Wang, C., Wang, Y. H., Liu, L., He, S. P., Li, R. S., Li, M., et al. (2014). The Paleoproterozoic magmatic–metamorphic events and cover sediments of the Tielik Belt and their tectonic implications for the southern margin of the Tarim Craton, northwestern China. *Precambrian Res.* 254, 210–225. doi:10.1016/j.precamres.2014.08.018
- Wang, J., Hattori, K., Liu, J. G., Song, Y., Gao, Y. B., and Zhang, H. (2017). Shoshonitic and adakitic magmatism of the early paleozoic age in the Western Kunlun orogenic belt, NW China: implications for the early evolution of the northwestern Tibetan plateau. *Lithos* 286, 345–362. doi:10.1016/j.lithos.2017.06.013
- Wang, W., Wang, J. X., Ma, H. D., Zhu, B. Y., and Liu, X. J. (2021). Mineralization age of the Karakorum Luobugaizi large lead-zinc deposit: the implication on exploration of Tianshuihai-Karakorum Super-large lead-zinc deposits. *Northwest. Geol.* 54 (03), 155–162. (in Chinese with English abstract). doi:10.19751/j.cnki.61-1149/p.2021.03.012
- We, C., Ye, L., Hu, Y. S., Huang, Z. L., Danyushevsky, L., and Wang, H. Y. (2021). LA-ICP-MS analyses of trace elements in base metal sulfides from carbonate-hosted Zn–Pb deposits, south China: a case study of the Maoping deposit. *Ore Geol. Rev.* 130, 103945. doi:10.1016/j.oregeorev.2020.103945
- Xiao, W. J., Windley, B. F., Liu, D. Y., Jian, P., Liu, C. Z., Yuan, C., et al. (2005). Accretionary tectonics of the Western Kunlun Orogen, China: a paleozoic–early Mesozoic, long-lived active continental margin with implications for the growth of Southern Eurasia. *J. Geol.* 113 (6), 687–705. doi:10.1086/449326
- Xiao, F., Lin, W. P., and Cheng, Q. M. (2023). *Ab-initio* calculations and molecular dynamics simulations of In, Ag, and Cu replacing Zn in sphalerite: implications for critical metal mineralization. *Ore Geol. Rev.* 163, 105699. doi:10.1016/j.oregeorev.2023.105699
- Xing, B., Mao, J. W., Xiao, X. N., Liu, H., Jia, F. D., Wang, S. S., et al. (2021). Genetic discrimination of the Dingjiashan Pb–Zn deposit, SE China, based on sphalerite chemistry. *Ore Geol. Rev.* 135, 104212. doi:10.1016/j.oregeorev.2021.104212
- Xu, S. Q., Feng, J., Tian, J. T., and Zhao, T. Y. (2013). Metallogenic rules and regional prediction of lead-zinc deposits in Luoshigou of West Kunlun. *J. Jilin Univ. Earth Sci. Ed.* 43 (4), 1190–1199. (in Chinese with English abstract). doi:10.13278/j.cnki.jjuese.2013.04.003
- Yan, C. H., Chen, C. J., Cao, X. Z., Zhang, W. S., Chen, J. K., Li, S. P., et al. (2012). The discovery of the “Pamir-type” iron deposits in Taxkorgan area of Xinjiang and its geological significance. *Geol. Bull. China* 31 (4), 549–557. (in Chinese with English abstract).
- Yang, Q., Zhang, X. J., Ulrich, T., Zhang, J., and Wang, J. (2022). Trace element compositions of sulfides from Pb–Zn deposits in the Northeast Yunnan and northwest Guizhou Provinces, SW China: insights from LA-ICP-MS analyses of sphalerite and pyrite. *Ore Geol. Rev.* 141, 104639. doi:10.1016/j.oregeorev.2021.104639
- Yang, F., Yin, J. Y., Xiao, W. J., Fowler, M., Kerr, A. C., Tao, Z. L., et al. (2024a). Early Cretaceous continental arc magmatism in the Wakhan Corridor, South Pamir: Mantle evolution and geodynamic processes during flat subduction of the Neo-Tethyan oceanic slab. *Geol. Soc. Am. Bull.* 136 (9–10), 4175–4194. doi:10.1130/B37411.1
- Yang, F. C., Romer, R. L., Glodny, J., and Li, W. C. (2024b). Magmatic evolution and sources of metals and fluids in the large granite-related Xiasai vein-type Ag–Pb–Zn (-Sn) deposit, northern Yidun terrane, SW China. *Ore Geol. Rev.* 171, 106183. doi:10.1016/j.oregeorev.2024.106183
- Ye, L., Cook, N. J., Ciobanu, C. L., Liu, Y. P., Zhang, Q., Liu, T. G., et al. (2011). Trace and minor elements in sphalerite from base metal deposits in South China: a LA-ICPMS study. *Ore Geol. Rev.* 39 (4), 188–217. doi:10.1016/j.oregeorev.2011.03.001
- Ye, L., Gao, W., Yang, Y. L., Liu, T. G., and Peng, S. S. (2012). Trace elements in sphalerite in Laochang Pb–Zn polymetallic deposit, Lancang, Yunnan province. *Acta Petrol. Sin.* 28 (5), 1362–1372. (in Chinese with English abstract).
- Ye, L., Li, Z. L., Hu, Y. S., Huang, Z. L., Zhou, J. X., Fan, H. F., et al. (2016). Trace elements in sulfide from the Tianbaoshan Pb–Zn deposit, Sichuan Province, China: a LA-ICPMS study. *Acta Petrol. Sin.* 32 (11), 3377–3393. (in Chinese with English abstract).
- Yu, H. T., Liu, J. S., Liu, W. H., Wang, T. G., and Li, X. (2013). Ore-controlling structure and metallogenic model of Kalayashake Pb–Zn–Cu polymetallic deposit in West Kunlun. *Glob. Geol.* 32 (04), 733–739+746. (in Chinese with English abstract).
- Yuan, B., Zhang, C. Q., Yu, H. J., Yang, Y. M., Zhao, Y. X., Zhu, C. C., et al. (2018a). Element enrichment characteristics: insights from element geochemistry of sphalerite in Daliangzi Pb–Zn deposit, Sichuan, Southwest China. *J. Geochem. Explor.* 186, 187–201. doi:10.1016/j.gexplo.2017.12.014
- Yuan, H. L., Liu, X., Chen, L., Bao, Z. A., Chen, K. Y., Zong, C. L., et al. (2018b). Simultaneous measurement of sulfur and lead isotopes in sulfides using nanosecond laser ablation coupled with two multi-collector inductively coupled plasma mass spectrometers. *J. Asian Earth Sci.* 154, 386–396. doi:10.1016/j.jseas.2017.12.040
- Zartman, R. E., and Doe, B. R. (1981). Plumbotectonics—The model. *Tectonophysics* 75 (1–2), 135–162. doi:10.1016/0040-1951(81)90213-4
- Zeng, Q. D., Wang, Z. C., He, H. Y., Wang, Y. B., Zhang, S., and Liu, J. M. (2014). Multiple isotope composition (S, Pb, H, O, He, and Ar) and genetic implications for gold deposits in the Jiapigou gold belt, Northeast China. *Min. Deposita* 49, 145–164. doi:10.1007/s00126-013-0475-2

- Zhang, Q. (1987). Trace elements in galena and sphalerite and their geochemical significance in distinguishing the genetic types of Pb-Zn ore deposits. *Chin. J. Geochem.* 6, 177–190. doi:10.1007/bf02872218
- Zhang, Z. W., Shen, N. P., Peng, J. T., Yang, X. R., Feng, G. Y., Fu, Y., et al. (2014). Syndeposition and epigenetic modification of the strata-bound Pb-Zn-Cu deposits associated with carbonate rocks in western Kunlun, Xinjiang, China. *Ore Geol. Rev.* 62, 227–244. doi:10.1016/j.oregeorev.2014.04.001
- Zhang, W. J., Wang, H., Yang, Y. F., and Sang, J. Z. (2018). Metallogenic characteristics of lead-zinc ore in Honghuangling, Hetian County, Xinjiang. *Geol. Explor.* 54 (S1), 1365–1372. (in Chinese with English abstract).
- Zhang, B. L., Wang, C. L., Robbins, L. J., Zhang, L. C., Konhauser, K. O., Dong, Z. G., et al. (2020a). Petrography and geochemistry of the Carboniferous Ortokarnash manganese deposit in the Western Kunlun Mountains, Xinjiang Province, China: implications for the depositional environment and the origin of mineralization. *Econ. Geol.* 115 (7), 1559–1588. doi:10.5382/econgeo.4729
- Zhang, H. S., Ji, W. H., Yang, X. Y., Zhou, J. X., Sun, C., Jia, Z. Y., et al. (2020b). The origin of the Quemuocuo carbonate-hosted Pb-Zn deposit in the Sanjiang Tethyan Belt, SW China: constrained by Sm-Nd isochronic age and Sr-S-Pb isotope compositions. *Ore Geol. Rev.* 117, 103264. doi:10.1016/j.oregeorev.2019.103264
- Zhang, C. L., Zou, H. b., and Liu, X. Q. (2022a). Cretaceous basalt-andesite sequence in the Southern Pamir: Arc—Back-arc architecture at the Pamir Plateau genetically related to the northward flat subductions of the Neo-Tethys Ocean. *Lithos* 422–423, 106747. doi:10.1016/j.lithos.2022.106747
- Zhang, J. K., Shao, Y. J., Liu, Z. F., and Chen, K. (2022b). Sphalerite as a record of metallogenic information using multivariate statistical analysis: constraints from trace element geochemistry. *J. Geochem. Explor.* 232, 106883. doi:10.1016/j.gexpro.2021.106883
- Zhao, X. J., Wu, Y. Z., Wang, T. S., Wang, X. A., Qiao, G. B., and Chen, D. H. (2014). Metallogenic characteristics and prospecting criteria of lead-zinc deposits in Qiao'er Tianshan-Chalukou region of West Kunlun. *Northwest. Geol.* 47 (04), 245–255. (in Chinese with English abstract).
- Zhao, H. T., Zhang, Y., Shao, Y. J., Liao, J., Song, S. L., Cao, G. S., et al. (2024). A new sphalerite thermometer based on machine learning with trace element geochemistry. *Nat. Resour. Res.* 33 (6), 2609–2626. doi:10.1007/s11053-024-10408-3
- Zhou, J. X., Huang, Z. L., Bao, G. P., and Gao, J. G. (2013a). Sources and thermo-chemical sulfate reduction for reduced sulfur in the hydrothermal fluids, southeastern SYG Pb-Zn metallogenic province, SW China. *J. Earth Sci.* 24 (5), 759–771. doi:10.1007/s12583-013-0372-8
- Zhou, J. X., Huang, Z. L., Zhou, M. F., Li, X. B., and Jin, Z. G. (2013b). Constraints of C-O-S-Pb isotope compositions and Rb-Sr isotopic age on the origin of the Tianqiao carbonate-hosted Pb-Zn deposit, SW China. *Ore Geol. Rev.* 53, 77–92. doi:10.1016/j.oregeorev.2013.01.001
- Zhou, J. X., Huang, Z. L., Lv, Z. C., Zhu, X. K., Gao, J. G., and Mirnejad, H. (2014). Geology, isotope geochemistry and ore genesis of the Shanshulin carbonate-hosted Pb-Zn deposit, southwest China. *Ore Geol. Rev.* 63, 209–225. doi:10.1016/j.oregeorev.2014.05.012
- Zhou, N. W., Chen, B. X., Deng, Z. F., Sang, M. S., and Bai, Q. J. (2019). Discovery and significance of early jurassic bimodal volcanic rocks in Huoshaoyun, Karakoram. *Geosci. Front.* 33 (05), 990–1002. doi:10.19657/j.geoscience.1000-8527.2019.05.06
- Zhu, Z. Y., Cook, N. J., Yang, T., Ciobanu, C. L., Zhao, K. D., and Jiang, S. Y. (2016). Mapping of sulfur isotopes and trace elements in sulfides by LA-(MC)-ICP-MS: potential analytical problems, improvements and implications. *Minerals* 6 (4), 110. doi:10.3390/min6040110
- Zhu, C. W., Wang, J., Zhang, J. W., Chen, X. C., Fan, H. F., Zhang, Y. X., et al. (2020). Isotope geochemistry of Zn, Pb and S in the ediacaran strata hosted Zn-Pb deposits in Southwest China. *Ore Geol. Rev.* 117, 103274. doi:10.1016/j.oregeorev.2019.103274
- Zhuang, L. L., Song, Y. C., Liu, Y. C., Fard, M., and Hou, Z. Q. (2019). Major and trace elements and sulfur isotopes in two stages of sphalerite from the world-class Angouran Zn-Pb deposit, Iran: implications for mineralization conditions and type. *Ore Geol. Rev.* 109, 184–200. doi:10.1016/j.oregeorev.2019.04.009